# Chapter 8
# Nonlinearities

**Antoine Chaigne, Joël Gilbert, Jean-Pierre Dalmont, and Cyril Touzé**

**Abstract** In the previous chapters, it was assumed that the amplitude of both air and structural oscillations in musical instruments were sufficiently small so that the assumption of linearity for their underlying models was fulfilled. However, this assumption is no longer valid in a number of situations encountered in musical acoustics, and a nonlinear approach becomes necessary for describing the observed phenomena. This chapter starts with the presentation of a simple example of nonlinear oscillator, the interrupted pendulum, whose aim is to introduce some fundamental properties of nonlinear systems, such as the dependence of resonance frequency on amplitude. The generic Duffing equation, which is found in many areas of nonlinear physics, is then examined. Musical applications are found first in piano strings, where the transverse-longitudinal coupling and the presence of additional partials in the spectrum (or "phantom" partials) are the consequence of nonlinearity due to high amplitude motion (geometric nonlinearity). In brass instruments, high values of the acoustic pressure induce nonlinear propagation which, in turn, might give rise to shock waves. In gongs and cymbals, a strong excitation produces the so-called bifurcations materialized by the emergence of new frequencies in the spectrum, which ultimately can lead to chaos. Specific methods are used for characterizing chaotic signals, such as the Lyapunov exponents. New emerging tools, such as the nonlinear normal modes (NNMs), appear to be very efficient for describing the dynamics of nonlinear systems with a reduced number of degrees of freedom. Self-sustained oscillations of reed, flute-like and bowed string instruments are treated in the three following chapters.

A. Chaigne (✉)
Institute of Music Acoustics, University of Music and Performing Arts Vienna (MDW), Anton-von-Webern-Platz 1, 1030 Vienna, Austria
e-mail: antchaigne@gmail.com

J. Gilbert • J.-P. Dalmont
Laboratoire d'Acoustique de l'Université du Maine (LAUM), Avenue Olivier Messiaen, 72085 Le Mans Cedex 09, France
e-mail: joel.gilbert@univ-lemans.fr; jean-pierre.dalmont@univ-lemans.fr

C. Touzé
Institute of Mechanical Sciences and Industrial Applications (IMSIA), ENSTA ParisTech, Université Paris-Saclay, 828 Boulevard des Maréchaux, 91762 Palaiseau Cedex, France
e-mail: cyril.touze@ensta-paristech.fr



A. Chaigne, J. Kergomard, *Acoustics of Musical Instruments*, Modern Acoustics and Signal Processing, DOI 10.1007/978-1-4939-3679-3_8

Most of the concepts on waves and modes presented in Parts I and II imply that the basic conditions of linearity are fulfilled. This requires first that the perturbations of the physical quantities involved in the models remain "small": there will be many opportunities to clarify what is meant by "small" in the following sections. The present chapter intends to show how to analyze and model the phenomena observed when the assumption of linearity is not valid anymore, which implies, in turn, that the effects of finite amplitude need to be considered (geometric nonlinearity). It is also important to know whether or not the constitutive equations of the materials remain linear. When stretching a rubber ribbon, for example, the relation between stress and strain significantly depends on the amplitude, even for a small tensile strength. This property is referred to as material nonlinearity.

Finally, and this is fundamental for the physics of musical instruments, the conditions for maintaining permanent oscillations in bowed stringed and wind instruments can be fulfilled only if a nonlinear element is introduced in the system loop. In fact, it would not be possible otherwise to transform a continuous source of energy, such as a static blowing pressure for the flute player, or a constant bow velocity for the violin player, into periodic oscillations. In this context, the purpose of the three following chapters is to give a detailed analysis of the instruments governed by self-sustained oscillations.

This chapter starts with the illustration of some fundamental concepts of geometric nonlinearity. Usual methods for studying nonlinear equations are introduced, including harmonic balance, iteration method, and the multiple scales method. Using simple examples, basic phenomena observed in nonlinear systems are introduced, such as eigenfrequencies depending on the amplitude, jumps, and hysteresis.

## 8.1 An Example of Asymmetry: The Interrupted Pendulum

First, a simple example of asymmetrical system is studied: the interrupted pendulum (see Fig. 8.1). The system is composed by a point mass $m$ suspended on a massless string of length $L$ at rest, attached to a pulley, and subjected to the action of gravity $g$. When the pendulum is set into motion, the string length changes over time: it increases when the weight moves away from the pulley of radius $R$, and it becomes shorter in the opposite case, when the string is wrapped around it. This elementary system illustrates several situations of asymmetry encountered in musical acoustics, for example, scrolling of the reed on the clarinet mouthpiece, boundary condition of a string on the tambura,[1] or geometric nonlinearity in gongs and cymbals (see Sect. 8.5). In the latter case, the curvature can be viewed as a stiffness asymmetry, where the rigid pulley adds some "stiffness" to the system during the time interval when the string is wrapped around it, compared to the free string case. This example is not only relevant in musical acoustics but also in other domains of physics. It has been used, for example, to understand complex nonlinear systems such as the propagation of compressional waves in rocks [22].

[1]The tambura is an Indian plucked stringed instrument.

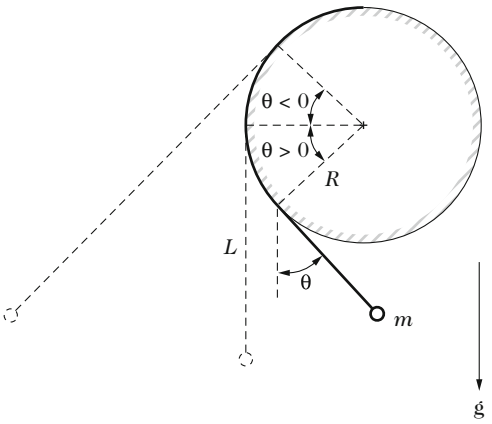


**Fig. 8.1** Interrupted pendulum (from Denardo [22]). A point mass $m$ is suspended to a massless string, forming a pendulum with a varying length during the motion due to the presence of the pulley which forms an obstacle

### 8.1.1 Equation of Motion

The equation of motion for the interrupted pendulum can be derived from the Lagrange equations [6]. The main variable is the angle $\theta$ made between the pendulum and the vertical axis. The instantaneous kinetic energy of the system is written $E_c = \frac{1}{2}m(L - R\theta)^2\dot{\theta}^2$. After some calculations, the equation of motion is found to be

$$\ddot{\theta} + \omega_0^2 \sin\theta = \rho\frac{d}{dt}(\theta\dot{\theta}), \tag{8.1}$$

where $\omega_o^2 = g/L$ and $\rho = R/L$. As $R$ tends to zero in (8.1), the well-known equation of a simple pendulum is found where the unique nonlinear term is $\sin\theta$. The right-hand side of the equation represents the nonlinearity introduced by the obstacle. Equation (8.1) is valid for $\theta \in [0, \theta_{\max}]$ where $\theta_{\max} = \min(1/\rho, \pi/2)$. In what follows, the pendulum is assumed to be released at the initial time ($t = 0$) from a position $\theta_0$ with zero initial velocity.

### 8.1.2 Solution by a Perturbation Method

For low and medium amplitudes, and with $\rho$ less than or equal to unity, it is observed experimentally that the solution is periodic (see Fig. 8.2) and that the period of the oscillation depends on the amplitude. It is also observed that the oscillation increasingly departs from the linear sinusoidal reference solution as the amplitude increases.

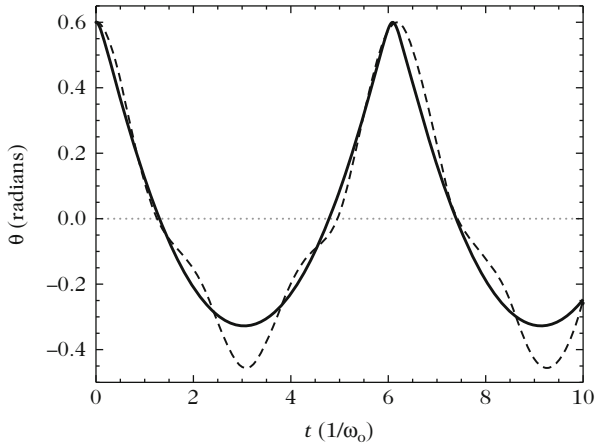


**Fig. 8.2** Oscillations of the interrupted pendulum (from Denardo [22]). Displacement waveform of the mass *m*. *Solid line*: exact solution. *Dashed line*: perturbative solution to the third order

These observations incite us to look for solutions under the following form:

$$\begin{cases} \theta = \varepsilon A \cos \omega t + \varepsilon^2 B \cos 2\omega t + \varepsilon^3 C \cos 3\omega t + \cdots = \varepsilon\theta_1 + \varepsilon^2\theta_2 + \varepsilon^3\theta_3 + \cdots, \\ \omega^2 = \omega_0^2 + \varepsilon\omega_1^2 + \varepsilon^2\omega_2^2 + \varepsilon^3\omega_3^2 + \cdots \end{cases} \tag{8.2}$$

In Eq. (8.2), the solution is written in terms of a Fourier series where the amplitudes of the respective coefficients are arranged in increasing powers of the dimensionless parameter $\varepsilon \ll 1$. Similarly, the oscillation frequency $\omega$ is expanded as a series of terms of increasing powers of $\varepsilon$ to account for variations with amplitude. The principle of the calculation consists in substituting the expansion (8.2) into (8.1) and in calculating the unknowns of the problem ($A$, $B$, $C$, $\omega_1$, $\omega_2$, $\omega_3$) separately [22]. For the sake of simplicity, the expansion is limited here to the third order in $\varepsilon$. In order to deal with dimensionless equations, the change of variable $\tau = \omega t$ is made.

Since the problem is of the third order, it is justified here to replace the term in $\sin\theta$ in (8.1) by the first two terms of its Taylor expansion: $\sin\theta \simeq \theta - \theta^3/6$. Equation (8.1) becomes

$$\omega^2 \frac{d^2\theta}{d\tau^2} + \omega_0^2 \left(\theta - \theta^3/6\right) = \rho\omega^2 \frac{d}{d\tau}\left(\theta \frac{d\theta}{d\tau}\right). \tag{8.3}$$

Inserting (8.2) in (8.3) and making the term $\varepsilon$ equals to zero, leads to

$$\frac{d^2\theta_1}{d\tau^2} + \theta_1 = 0, \tag{8.4}$$

which has a solution of the form $\theta_1 = A\cos\tau$, in view of the initial conditions. Setting the term in $\varepsilon^2$ to zero, we have

$$\frac{d^2\theta_2}{d\tau^2} + \theta_2 = \frac{\omega_1^2}{\omega_0^2}\theta_1 + \rho\frac{d}{d\tau}\left(\theta_1\frac{d\theta_1}{d\tau}\right). \tag{8.5}$$

By replacing the angular variables by their approximate expressions, one finds that Eq. (8.5) provides the following relation between the parameters:

$$-3B\cos 2\tau = \frac{\omega_1^2}{\omega_0^2}A\cos\tau - \rho A^2\cos 2\tau. \tag{8.6}$$

The basic principle of the method is then to set to zero the respective terms of each *harmonic* $n\tau$ (*harmonic balance*), which gives here:

$$\omega_1 = 0 \quad \text{and} \quad B = \frac{\rho A^2}{3}. \tag{8.7}$$

At this stage, one can check that Eq. (8.1) suggests that the obstacle formed by the pulley of radius $R$ causes a quadratic nonlinearity since an harmonic of order two is exhibited. This effect disappears if $\rho = 0$, i.e., without any obstacle. However, this nonlinearity causes no change in the angular frequency, at least at the first order. Continuing further by eliminating the terms of power 3 in $\varepsilon$, we get

$$\frac{d^2\theta_3}{d\tau^2} + \theta_3 = \frac{\omega_2^2}{\omega_0^2}\theta_1 + \frac{\theta_1^3}{6} + \rho\frac{d^2}{d\tau^2}(\theta_1\theta_2). \tag{8.8}$$

Replacing, as previously, the angular variables by their approximate expressions in (8.8), and eliminating further the terms in $n\tau$, leads to:

$$C = \frac{A^3}{192}\left(36\rho^2 - 1\right) \quad \text{and} \quad \frac{\omega_2^2}{\omega_0^2} = \frac{A^2}{24}\left(4\rho^2 - 3\right). \tag{8.9}$$

Finally, defining $\theta_{10} = \varepsilon A$ as the fundamental amplitude of the oscillation, the solution to the problem is written at the order 3:

$$\begin{cases} \theta = \theta_{10}\cos\omega t + \dfrac{\rho\theta_{10}^2}{3}\cos 2\omega t + (36\rho^2 - 1)\dfrac{\theta_{10}^3}{192}\cos 3\omega t, \\ \text{and} \\ \omega^2 = \omega_o^2\left[1 + \dfrac{\theta_{10}^2}{24}\left(4\rho^2 - 3\right)\right]. \end{cases} \tag{8.10}$$

This result suggests the following comments:

- At the third order, the fundamental amplitude is linked to the initial condition by the relation:

$$\theta_0 \simeq \theta_{10} + \frac{\rho\theta_{10}^2}{3} + (36\rho^2 - 1)\frac{\theta_{10}^3}{192}. \tag{8.11}$$

- Figure 8.2 shows that the third-order approximation yields a fair estimation of the oscillation period and waveform when $\theta$ is positive, i.e., when the string is in contact with the obstacle. However, it is necessary to expand the solution to higher orders in order to account for the observed oscillation when $\theta$ is negative.
- When $\rho = 0$, we have $\omega \simeq \omega_0(1 - \theta_{10}^2/16)$, and the term in $\cos 2\omega t$ is equal to zero. This yields a case of cubic nonlinearity due to gravity, through the term in $\sin\theta$. The tension of the string decreases as the amplitude of the motion increases, and it vanishes when the string reaches the horizontal plane, which corresponds to a decrease in the overall stiffness of the system.
- For $0 < \rho < \sqrt{3}/2$, the frequency decreases with the amplitude of the oscillation. The oscillator is said to show a *softening* behavior.
- For $\rho > \sqrt{3}/2$, the oscillator is of the *hardening* type. The stiffness provided by the obstacle becomes larger than the increase in softness due to gravity.
- When $\rho = \sqrt{3}/2$, the period of the oscillation is independent of the amplitude. This gives the particular case of an *isochronous pendulum*. This result remains true to the fourth order, since $\omega_3^2 = 0$ in the series expansion of $\omega^2$. Both softening and hardening effects are compensating one another.

In conclusion, it can be noticed that most nonlinear phenomena exhibited in this simple example also occur in more complex systems: frequency dependence with regard to the amplitude, softening or hardening behavior of some structural modes, etc. The method presented to solve this particular case is also applicable to other nonlinear systems. Gilbert et al. used a similar approach, for example, to predict the steady-state amplitude of sound pressure in a clarinet [29]. Before studying specific nonlinear phenomena of musical acoustics in subsequent sections more closely, the Duffing equation will first be examined in detail, as it is an equation frequently encountered in nonlinear dynamics.

## 8.2 Duffing Equation

Duffing equation is a generic nonlinear equation of an oscillator which includes a cubic term. It is found in many areas of physics, and therefore it has been the subject of extensive study. In mechanics, it is a good model for phenomena that occur for large amplitude oscillations when the elastic restoring force can no longer be considered as proportional to the displacement. In musical acoustics, this model is used for explaining the presence of phantom partials in the spectrum of piano strings, and the enrichment of spectrum due to increasing amplitudes in gongs and cymbals, as it will be seen later in this chapter.

The main properties of the Duffing equation will be first illustrated from the example of the elastic pendulum. This example can be considered as a simplified case, with one degree of freedom, of the increase in stiffness due to the extension of length in vibrating strings (see Sect. 8.3).

Another type of nonlinear equation frequently encountered in physics is the Van der Pol equation. It differs from Duffing equation by the fact that the nonlinearity is included in the dissipative term, and not in the stiffness term. It can lead to self-sustained oscillations, which correspond to oscillations that occur without an oscillating forcing term. The Van der Pol equation is not studied in this chapter, but it will serve as a basic simplified model of some instruments, such as the clarinet, and treated in detail in Chap. 9.

### 8.2.1 Example

Let us now consider the oscillator drawn in Fig. 8.3. The rigid mass $M$ is moved horizontally apart of a distance $x$ from its initial equilibrium position, under the effect of a sinusoidal force $F\cos\Omega t$. This mass is attached to two springs of stiffness $k$, with free length $L_0$. This length becomes equal to $L$ after stretching at rest. We denote $\lambda = L_0/L < 1$ and $y = x/L$.

During the motion, the spring length becomes $\ell(y) = L\sqrt{1+y^2}$ and the elastic potential energy stored in each spring is $\mathscr{E}_p = \frac{1}{2}k(\ell - L_0)^2$. Differentiating this expression with respect to $y$, the expression of the elastic restoring force exerted on the spring is obtained, from which the equation of motion is derived:

$$M\frac{d^2y}{dt^2} + 2ky\left[1 - \frac{\lambda}{\sqrt{1+y^2}}\right] = \frac{F}{L}\cos\Omega t. \tag{8.12}$$

Under the assumption of "small" displacements ($y \ll 1$), and setting $\omega_0^2 = 2k/M$, we obtain a first-order approximation:

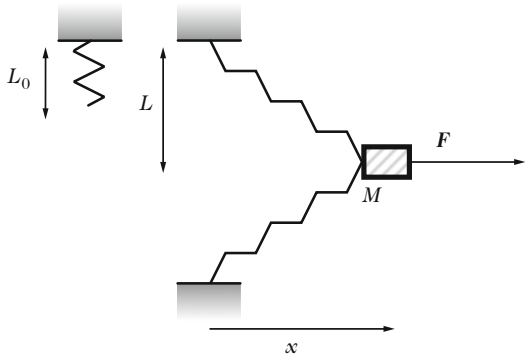


**Fig. 8.3** Elastic pendulum

$$\frac{d^2y}{dt^2} + \omega_0^2(1-\lambda)y + \frac{\omega_0^2\lambda}{2}y^3 = \frac{F}{ML}\cos\Omega t, \tag{8.13}$$

or, equivalently, in dimensionless form, with $\tau = \omega t$, $\omega^2 = \omega_0^2(1-\lambda)$ and $\gamma = \Omega/\omega$:

$$\frac{d^2y}{d\tau^2} + y + \eta y^3 = \alpha\cos\gamma\tau, \tag{8.14}$$

where $\eta = \frac{\lambda}{2(1-\lambda)}$ and $\alpha = \frac{F}{ML\omega^2}$. Equation (8.14) is a Duffing equation with a forcing term. In the example above, the coefficient $\eta$ is positive. An equation similar to the case of the interrupted pendulum is obtained (with $R = 0$ and $\theta$ small), though with a change of sign for $\eta$.

### 8.2.2 Solutions for the Forced Duffing Oscillator

In what follows, both coefficients $\eta$ and $\alpha$ defined in (8.14) are assumed to be small compared to unity. In addition, $\eta$ is positive (equivalent to $\lambda \ll 1$ in the previous example), which corresponds to the case of an *hardening* oscillator. The Duffing equation is solved by the *iteration method*, whose principle is to look for step-by-step refined approximations of the solution. Considering the solution obtained in the case of the linear oscillator (see Chap. 2), the solution $y_1(t) = A\cos\gamma\tau$ is selected as a starting approximation, where $A$ is the unknown. The coefficient $A$ can be positive or negative, depending on whether the solution is in phase or in antiphase with the force. The approximation of order 2 is sought in the form:

$$y_2(\tau) = A\cos\gamma\tau + B\cos 3\gamma\tau. \tag{8.15}$$

Now, $y_2$ is inserted in (8.14). Using the trigonometric identity

$$4\cos^3\gamma\tau = 3\cos\gamma\tau + \cos 3\gamma\tau, \tag{8.16}$$

and writing down the condition for which the amplitude of the term $\cos\gamma\tau$ is equal to zero, we have

$$(1-\gamma^2)A + \frac{3\eta A^3}{4} = \alpha. \tag{8.17}$$

**Note** To obtain the amplitude $B$ of the term $\cos 3\gamma\tau$, the calculation must be continued with an approximation of order 3, and so on.

If the nonlinearity coefficient $\eta$ is equal to zero in (8.17), then the resonance curve of the linear oscillator in forced oscillations is found: $A = \frac{\alpha}{1-\gamma^2}$, or, equivalently,

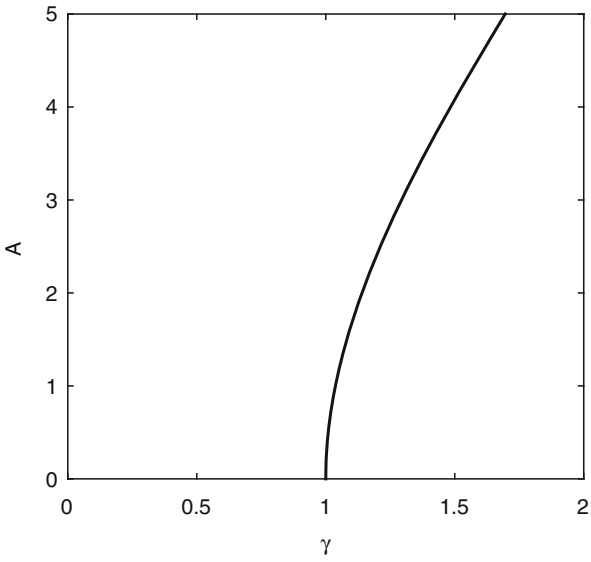


**Fig. 8.4** Backbone curve for the Duffing equation with $\eta > 0$; $\gamma = \Omega/\omega$

$X = AL = \frac{F}{M}\frac{1}{\omega^2 - \Omega^2}$ using the dimensional quantities. Another method for obtaining the result (8.17) will be presented later in this chapter. To plot the resonance curves in the general case, it is convenient to write (8.17) under the form

$$\gamma^2 - 1 = \frac{3\eta A^2}{4} \pm \frac{\alpha}{|A|}. \tag{8.18}$$

- When $\alpha = 0$, the limiting case (the so-called backbone curve) is obtained (see Fig. 8.4). In the quarter plane ($\Omega^2 > 0, |A| > 0$), this curve is parabola with its concavity facing upwards, which corresponds here to the *hardening* case, i.e., to an increase of frequency with amplitude.
- When $\alpha \neq 0$, two branches of solution are obtained depending on whether $A$ is positive or negative. In the first case, the resonance curve is located above the parabola. In the second case, it is located below.

To find the standard resonance curves, the $x$-axis and $y$-axis need to be reversed, after calculating the square root of $\Omega^2$. If $\eta < 0$, the limiting curve of free oscillations in the quarter plane ($\Omega^2 > 0, |A| > 0$) is a parabola of concavity facing downwards, which corresponds to the case of a *softening* oscillator, where the eigenfrequency decreases with amplitude. With $\alpha \neq 0$, both branches of the curve are obtained with (8.18). If a viscous damping is introduced in the Duffing equation, it can be written in dimensionless form:

$$\frac{d^2y}{d\tau^2} + \beta\frac{dy}{d\tau} + y + \eta y^3 = \alpha \cos \gamma\tau. \tag{8.19}$$

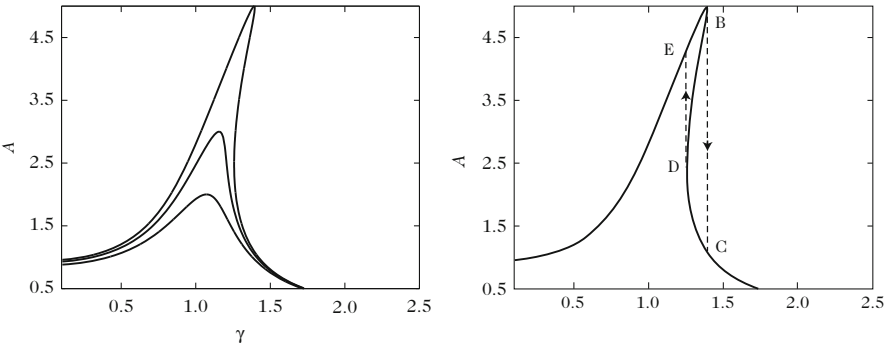


**Fig. 8.5** (*Left*) Resonance curves of the damped Duffing equation for different values of the damping: the bending of the curves is more pronounced for low damping. (*Right*) Hysteresis loop: when $\gamma$ increases, the operating point jumps from B to C; when $\gamma$ decreases, the operating point jumps from D to E

With a similar approach as above, it is found that the resonance curves are governed by the equation:

$$\left[(1-\gamma^2)A + \frac{3\eta A^3}{4}\right]^2 + \beta^2 A^2 = \alpha^2 \tag{8.20}$$

which corresponds to the curves shown in Fig. 8.5.

#### 8.2.2.1 Jump and Hysteresis Phenomena

The resonance curves of the nonlinear Duffing oscillator are bent to the left or to the right (see Fig. 8.5). As a consequence, a frequency domain exists (delimited by dotted lines in the figure) where one value of $\gamma$ may correspond to three values of $|A|$. Through a rigorous mathematical reasoning, it can be shown that the extreme values obtained for $|A|$ are stable, while the states corresponding to the middle curve portion are unstable. In Sect. 8.5.4.1, a general method for determining the stability of oscillators will be studied. Experimentally, the consequences of these stability properties are the following:

1. If the frequency increases (resp. decreases) regularly, the intersection point in the middle curve does not stay fixed, and it "jumps" from one stable curve to the other as soon as the point on one stable curve reaches its limit (see Fig. 8.5).
2. The closed curve built up by the two jumps and the two stable portions of both upper and lower curves forms a *hysteresis loop*.

#### 8.2.2.2 Secular Terms

Let us now return to the generic Duffing equation under forced oscillations, written in dimensionless form as follows:

$$\ddot{q} + q + \varepsilon q^3 = F \cos \Omega t, \tag{8.21}$$

with

$$F = \varepsilon F_0, \ \Omega^2 = 1 + \varepsilon \omega_1^2. \tag{8.22}$$

**Note** With these notations, all quantities $q$ (and its derivatives), $F$, $\Omega$ are dimensionless. Thus, the eigenfrequency of the linear oscillator is now denoted 1 instead of $\omega_0$. The dimensionless parameter $\omega_1$ quantifies the difference between the oscillator's eigenfrequency and the forcing frequency. The expressions (8.22) indicate first that the study is restricted here to forcing frequencies close to the oscillator's eigenfrequency and, secondly, that the forcing amplitude is low.

Let us look for solutions in the form of an expansion in $\varepsilon$, as in the case of free oscillations for the interrupted pendulum:

$$q(t) = q_0(t) + \varepsilon q_1(t) + \cdots \tag{8.23}$$

By replacing the quantity $q$ by its first-order expansion, we have

$$\ddot{q}_0 + \varepsilon \ddot{q}_1 + \left(\Omega^2 - \varepsilon \omega_1^2\right)(q_0 + \varepsilon q_1) + \varepsilon (q_0 + \varepsilon q_1)^3 = \varepsilon F_0 \cos \Omega t. \tag{8.24}$$

At zero order, this yields immediately

$$\ddot{q}_0 + \Omega^2 q_0 = 0, \tag{8.25}$$

from which we derive $q_0(t) = A \cos \Omega t$. At the order one, we have

$$\ddot{q}_1 + \Omega^2 q_1 = \left[\left(\omega_1^2 - \frac{3}{4}A^2\right)A + F_0\right] \cos \Omega t - \frac{1}{4}A^3 \cos 3\Omega t. \tag{8.26}$$

Here, the important point to consider is that an equation is obtained where the frequency of one forcing term (at the right-hand side) is equal to the oscillator eigenfrequency $\Omega$. As shown in the first part of this book, this resonance case leads to an continuous increase of the amplitude of the solution with time, in $t \cos \Omega t$. These terms, called secular terms,[2] must be eliminated here, since stationary

[2]The origin of this denomination is due to the fact that these terms were highlighted as first in the field of celestial mechanics, where the time scales are of the order of centuries rather than of milliseconds!

solutions are sought. The amplitude of the term $\cos \Omega t$ in the right-hand side is thus put equal to zero, which leads to the condition

$$\left(\omega_1^2 - \frac{3}{4}A^2\right)A + F_0 = 0, \tag{8.27}$$

and, in turn, to the relation between amplitude and forcing parameters

$$\frac{3}{4}\varepsilon A^3 - A(\Omega^2 - 1) = F. \tag{8.28}$$

In conclusion, the result obtained for the forced spring pendulum in Eq. (8.17) is found again here, though with another method. For a forcing amplitude equal to zero ($F = 0$), the case of free oscillations is recognized. With $\varepsilon = 0$, we obtain the linear case.

### 8.2.3 Generation of Subharmonics

Nonlinear oscillators have the property to generate spectral components which are not included in the excitation spectrum. This section examines under which conditions a Duffing oscillator subjected to forced oscillations can generate subharmonics, i.e., spectral components of frequency equal to a submultiple of the excitation frequency or, equivalently, whose period is a multiple of the forcing period. Let us consider the forced Duffing equation with a source term of reduced frequency $3\gamma$ :

$$\frac{d^2y}{d\tau^2} + y + \eta y^3 = \alpha \cos 3\gamma\tau, \tag{8.29}$$

with $\eta \ll 1$. We look for the solutions that can be expanded in the form:

$$y(\tau) = y_0(\tau) + \eta y_1(\tau) \quad \text{with} \quad \gamma^2 = 1 + \eta\gamma_1^2. \tag{8.30}$$

Inserting the expressions (8.30) in (8.29), and eliminating the terms of order 2 in $\eta$ (and higher), we get

$$\frac{d^2y_0}{d\tau^2} + \gamma^2 y_0 - \eta\gamma_1^2 y_0 + \eta\frac{d^2y_1}{d\tau^2} + \eta\gamma^2 y_1 + \eta y_0^3 = \alpha \cos 3\gamma\tau. \tag{8.31}$$

The linear solution (term of order 0) is obtained by setting $\eta = 0$ in (8.31) which yields

$$\frac{d^2y_0}{d\tau^2} + \gamma^2 y_0 = \alpha \cos 3\gamma\tau, \tag{8.32}$$

which, under the additional assumption of zero initial velocity, leads to a solution of the form $y_0(\tau) = A\cos\gamma\tau + C\cos 3\gamma\tau$. Finally, inserting the latter expression in (8.32) leads to $C = -\frac{\alpha}{8\gamma^2}$.

In the next step, the term in $\eta$ is set to zero in (8.31), to ensure compatibility of the equation, which provides the term of order 1 of the solution:

$$\frac{d^2y_1}{d\tau^2} + \gamma^2 y_1 = \gamma_1^2 y_0 - y_0^3. \tag{8.33}$$

Now, by substituting in (8.33) the expression for $y_o(\tau)$, and after some trigonometric calculations, it is found that $y_1(\tau)$ must satisfy the equation:

$$\begin{aligned}\frac{d^2y_1}{d\tau^2} + \gamma^2 y_1 = A\left[\gamma_1^2 - \frac{3}{4}\left(A^2 + \frac{3\alpha^2}{64\gamma^4} - \frac{A\alpha}{8\gamma^2}\right)\right]\cos\gamma\tau \\ + \text{ terms in } 3\gamma,\ 5\gamma,\ 7\gamma,\ 9\gamma.\end{aligned} \tag{8.34}$$

Equation (8.34) shows that if the forcing amplitude of the $\gamma$ term is not equal to zero, then we again face a situation where the amplitude of an oscillator, excited at its eigenfrequency, increases continuously in time. After removing the secular terms, we get

$$\gamma_1^2 = \frac{3}{4}\left(A^2 + \frac{3\alpha^2}{64\gamma^4} - \frac{A\alpha}{8\gamma^2}\right). \tag{8.35}$$

After some algebraic rearrangement, Eq. (8.35) provides the condition of existence for subharmonics of order 3 in the form of a relation between the amplitude $A$ and the reduced frequency $\gamma$, for a given cubic nonlinearity coefficient $\eta$:

$$\gamma^6 - \gamma^4 - \frac{3\eta}{256}\left(64A^2\gamma^4 - 8A\alpha\gamma^2 + 2\alpha^2\right) = 0. \tag{8.36}$$

Finally, let us indicate that any oscillator governed by the Duffing equation may also exhibit *harmonics of higher order*. To demonstrate this, the previous calculation must be carried out again, with an forcing term in $\gamma$, and with the objective of obtaining conditions of existence for solutions in $3\gamma$ (or higher).

## 8.3 Nonlinear Vibrations of Strings

The models of strings presented in the previous chapters do not take the variations of tension consecutive to length fluctuations during the motion into account. This assumption is not justified anymore when the ratio between the transverse displacement and the string's length becomes large. In several stringed instruments (electric guitar, gypsy guitar, double bass played pizzicato,...) such variations of

tension are responsible for perceptually and musically relevant nonlinear effects: pitch glide (think of the well-known initial "twang" in the attack!), coupling between modes, and elliptical polarization of the string. One particular effect of nonlinear coupling between modes lies in the ability to excite a string at a fraction $L/n$ of its length without canceling the harmonics of order $n$, in contradiction with the linear theory. The elliptical polarization of a string also is a consequence of the nonlinearity due to variations of tension.

The forced vibrations of an elastic string are examined below for large amplitude oscillations. These will be focused on two transverse components of the string's motion, denoted $y(x,t)$ and $z(x,t)$. Torsional vibrations and longitudinal vibrations are ignored [49, 73]. One may refer to the paper by Watzky for a more complete description of the nonlinear dynamics of a vibrating string [75].

### 8.3.1 Simplified Equations of Motion

Let $T_0$ be the initial tension of the string at rest. During the string motion, the relative increase in length $\lambda$ of a small element of initial length $dx$ is given by:

$$ds - dx = \lambda dx, \tag{8.37}$$

where $ds$ is the current length (at time $t$) of the element (see Fig. 8.6).

For an elastic string of Young's modulus $E$ and cross-section $A$ (in $m^2$), the tension at time $t$ during the motion becomes

$$T = T_0 + EA\lambda\,. \tag{8.38}$$

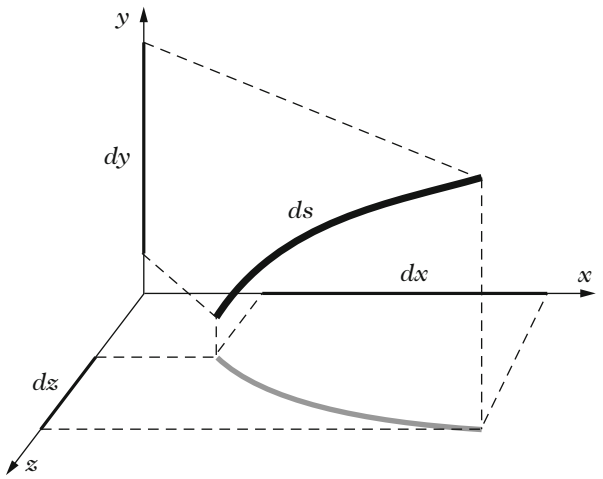


**Fig. 8.6** Geometry of a nonlinear string element

It is assumed that the components of the strain tensor (see Chap. 1) remain small compared to unity so that it can be written that $ds = [dx^2 + dy^2 + dz^2]^{1/2}$. A second-order Taylor expansion of this equation gives

$$ds = dx \left\{ 1 + \frac{1}{2} \left[ \left( \frac{\partial y}{\partial x} \right)^2 + \left( \frac{\partial z}{\partial x} \right)^2 \right] - \frac{1}{8} \left[ \left( \frac{\partial y}{\partial x} \right)^2 + \left( \frac{\partial z}{\partial x} \right)^2 \right]^2 + \cdots \right\}. \tag{8.39}$$

Inserting this expression in (8.38) and assuming also that $EA \gg T_0$, it can be shown that the potential energy of the string of length $L$ fixed rigidly at both ends is written [49]:

$$E_p = \int_0^L \left\{ \frac{T_0}{2} \left[ \left( \frac{\partial y}{\partial x} \right)^2 + \left( \frac{\partial z}{\partial x} \right)^2 \right] + \frac{EA}{8} \left[ \left( \frac{\partial y}{\partial x} \right)^2 + \left( \frac{\partial z}{\partial x} \right)^2 \right]^2 \right\} dx. \tag{8.40}$$

The kinetic energy is written:

$$E_c = \frac{\mu}{2} \int_0^L \left[ \left( \frac{\partial y}{\partial t} \right)^2 + \left( \frac{\partial z}{\partial t} \right)^2 \right] dx. \tag{8.41}$$

By using the Hamilton's principle, and considering that a sinusoidal force $f(x) \cos \omega t$ is applied to the string in the transverse direction $y$, the following coupled equations are obtained (where the subscript letters refer to partial derivatives):

$$\begin{cases} y_{tt} - c_o^2 y_{xx} = \dfrac{c_1^2}{2} \left[ 3 y_{xx} y_x^2 + \dfrac{\partial}{\partial x} (y_x z_x^2) \right] + \dfrac{f(x)}{\mu} \cos \omega t, \\ z_{tt} - c_o^2 z_{xx} = \dfrac{c_1^2}{2} \left[ 3 z_{xx} z_x^2 + \dfrac{\partial}{\partial x} (z_x y_x^2) \right], \end{cases} \tag{8.42}$$

where $c_o = \sqrt{T_0/\mu}$ and $c_1 = \sqrt{EA/\mu}$ are the transverse and longitudinal velocities in the linear case, respectively. In Eq. (8.42) the left-hand sides correspond to the linear case, while nonlinear terms are the terms in brackets on the right-hand side. These terms can be ignored as long as the gradients $y_x$ and $z_x$ remain weak. Otherwise, they are responsible for a coupling between $y$ and $z$. Thus, a force applied in the direction $y$ is likely to generate a motion in the perpendicular direction $z$. This explains why an initially plane motion of the string does not remain plane during the motion.[3]

[3] Let us recall (see Chap. 6) that the boundary conditions at the bridge are another cause of coupling between $y$ and $z$ in the linear case. In the general complex case of a real stringed instrument during normal playing, these two factors coexist and it is often difficult to separate them.

### 8.3.2 *Forced Vibrations*

As a result of the large amplitude displacement of the string, it is usually not justified to neglect the nonlinear terms in (8.42) close to resonances. In what follows, it is assumed that the forcing frequency $\omega$ is close to one particular eigenfrequency $\omega_n = \frac{n\pi c_0}{L}$ of the string. It is further assumed, for simplicity, that the mode $n$ is not coupled to other modes, which is not the case in practice. In fact, if the modes are close together and/or if there are some algebraic relations between the eigenfrequencies (see below, Sect. 8.5), then intermodal coupling must be taken into account. To a first approximation, let us consider the two transverse components of the string for the mode $n$:

$$y(x,t) = a_{ny} \sin \frac{n\pi x}{L} \cos \omega t \quad \text{and} \quad z(x,t) = a_{nz} \sin \frac{n\pi x}{L} \sin \omega t. \tag{8.43}$$

Inserting the expressions (8.43) in (8.42), the amplitudes $a_{ny}$ and $a_{nz}$ satisfy the following relations:

$$\begin{cases} (\omega_n^2 - \omega^2) a_{ny} + \dfrac{9c_1^2}{32} \left(\dfrac{n\pi}{L}\right)^4 a_{ny}^3 + \dfrac{3c_1^2}{32} \left(\dfrac{n\pi}{L}\right)^4 a_{ny} a_{nz}^2 = \dfrac{\alpha_n}{\mu}, \\ (\omega_n^2 - \omega^2) a_{nz} + \dfrac{9c_1^2}{32} \left(\dfrac{n\pi}{L}\right)^4 a_{nz}^3 + \dfrac{3c_1^2}{32} \left(\dfrac{n\pi}{L}\right)^4 a_{nz} a_{ny}^2 = 0, \end{cases} \tag{8.44}$$

where $\alpha_n$ is the projection of the excitation force on the mode $n$ of the string.

#### 8.3.2.1 Planar Motion

The case of a planar motion is obtained by setting $a_{nz} = 0$ in (8.44). In this case, the amplitude in the $y$-direction is governed by the nonlinear equation:

$$(\omega_n^2 - \omega^2) a_{ny} + \frac{9c_1^2}{32} \left(\frac{n\pi}{L}\right)^4 a_{ny}^3 = \frac{\alpha_n}{\mu}, \tag{8.45}$$

which is similar to Eq. (8.17) obtained for a Duffing oscillator under forced oscillations. Therefore, all results presented in Sect. 8.2.2 for Duffing oscillators of "hardening" type are valid here, including bending of resonance curves, jumps, and hysteresis.

#### 8.3.2.2 Out-of-Plane Motion

Eliminating $a_{nz}$ between both Eq. (8.44), yields for $a_{ny}$:

$$(\omega_n^2 - \omega^2) a_{ny} + \frac{3c_1^2}{8} \left(\frac{n\pi}{L}\right)^4 a_{ny}^3 = \frac{\alpha_n}{\mu}. \tag{8.46}$$

This expression is similar to (8.45), though the nonlinear term is now multiplied by a factor $4/3$, compared to the case of a planar motion. The second equation becomes

$$a_{nz}^2 = a_{ny}^2 - \frac{16}{3}\frac{\alpha_n}{\mu c_1^2 \left(\frac{n\pi}{L}\right)^4 a_{ny}}. \tag{8.47}$$

It proves that the string is likely to have an elliptical motion at a given point of abscissa $x$, under the condition:

$$a_{ny} > a_{ny}^{\text{crit}} = \left[\frac{16\alpha_n}{3\mu c_1^2 \left(\frac{n\pi}{L}\right)^4}\right]^{1/3}. \tag{8.48}$$

The condition (8.48) shows that increasing the forcing amplitude facilitates the emergence of such motion. For plucked, and struck, string instruments, the elliptical polarization has important consequences on the sound. In fact, each polarization is "loaded" by a specific impedance at the bridge. Consequently, the detuning and damping of both polarizations, due to these boundary conditions, are slightly different. This, in turn, induces beats and complex decay history, which are particularly sensitive to the attack time, when the amplitude is the largest. In the spectral domain, these nonlinear phenomena take the form of "double peaks" of very close frequencies.

In conclusion, it has been shown here that a single nonlinear string shows some characteristics observed in the case of linear coupled strings in pianos (see Chap. 6). However, it is important to notice that the underlying physical phenomena at the origin of these temporal and spectral properties are fundamentally different: amplitude nonlinearity in the first case, moving end in the linear case. Both phenomena exist in the vibrations of real piano strings, so that it is sometimes hard to separate them experimentally.

### *8.3.3 Transverse-Longitudinal Coupling: Simplified Approach*

In the previous section, the coupling between transverse and longitudinal motion of the string is ignored. However, in many string instruments and, in particular, in pianos, such coupling is clearly visible and has a perceptual relevance [15]. To illustrate this, Fig. 8.7 shows the recorded acceleration at the bridge of a piano. It highlights the existence of the so-called precursor, that precedes the transverse vibration. Spectral analysis of this precursor shows that it is mainly due to longitudinal vibration of the string, caused by its elongation during the attack [2].

This section is dedicated to the analysis of this coupling. It is restricted to the description of the coupling between one transverse polarization $y(x,t)$ and the longitudinal (or axial) motion $\xi(x,t)$. The string is assumed to be homogeneous, lossless, and rigidly fixed at both ends. Finally, it is assumed that both transverse

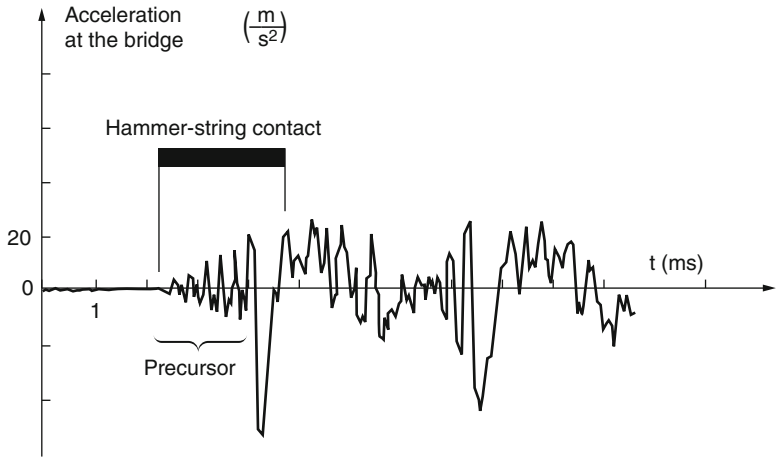


**Fig. 8.7** Acceleration at the bridge of a piano. A precursor is clearly visible in the initial part of the waveform. It is due to the longitudinal vibration of the string struck by the hammer. The duration of hammer-string contact is indicated by a *black rectangle*, for comparison. From [2]

and longitudinal modes are integer multiples of their respective fundamentals. The proposed approach used below is close to the one used by Bank [7], and inspired by Morse [46]. We start from Eq. (8.38) where the extension d$s$, for a given axial displacement $\xi(x,t)$, is written:

$$\mathrm{d}s = dx\sqrt{\left(1+\frac{\partial\xi}{\partial x}\right)^2+\left(\frac{\partial y}{\partial x}\right)^2}, \tag{8.49}$$

from which a first-order expression of string tension is derived

$$T = T_0 + EA\left[\frac{\partial\xi}{\partial x}+\frac{1}{2}\left(\frac{\partial y}{\partial x}\right)^2\right]. \tag{8.50}$$

Thus the longitudinal force exerted on the string element $ds$ is written:

$$F_x = \frac{\partial T}{\partial x}dx = EA\left[\frac{\partial^2\xi}{\partial x^2}+\frac{1}{2}\frac{\partial}{\partial x}\left(\frac{\partial y}{\partial x}\right)^2\right]dx. \tag{8.51}$$

This yields the equation that governs the longitudinal displacement of the string:

$$\mu\frac{\partial^2\xi}{\partial t^2} = EA\left[\frac{\partial^2\xi}{\partial x^2}+\frac{1}{2}\frac{\partial}{\partial x}\left(\frac{\partial y}{\partial x}\right)^2\right]. \tag{8.52}$$

The equation that governs the transverse string component $y$ is written:

$$\mu \frac{\partial^2 y}{\partial t^2} = T_0 \frac{\partial^2 y}{\partial x^2} + EA \frac{\partial}{\partial x} \left\{ \frac{\partial y}{\partial x} \left[ \frac{\partial \xi}{\partial x} + \frac{1}{2} \left( \frac{\partial y}{\partial x} \right)^2 \right] \right\}. \tag{8.53}$$

It should be noticed in Eq. (8.52) that the coupling term due to transverse motion is quadratic in $y$, while in (8.53) the coupling term due to longitudinal motion is cubic in $y$. Under the assumptions of fixed boundary conditions and homogeneous string, the transverse motion is expanded in the form:

$$y(x,t) = \sum_{n=1}^{\infty} y_n(t) \sin \frac{n\pi x}{L}. \tag{8.54}$$

At this step, the goal is to define the conditions of existence for longitudinal motion of the string and quantify it (this will be referred to as transverse-longitudinal, or TL, mode coupling). The inverse problem, namely the generation of a transverse motion induced by a longitudinal motion (longitudinal-transverse, or LT, mode coupling) is intentionally left aside. Both couplings exist simultaneously in reality, but the description of the TL coupling is sufficient to bring out the essential principles. Starting from (8.54), the longitudinal force per unit length of the string is written, from (8.51)

$$\begin{aligned} f_{\mathrm{TL}}(x,t) &= \frac{EA}{2} \frac{\partial}{\partial x} \left( \frac{\partial y}{\partial x} \right)^2 = \frac{EA}{2} \frac{\partial}{\partial x} \left[ \sum_{n=1}^{\infty} y_n(t) \frac{n\pi}{L} \cos \frac{n\pi x}{L} \right]^2 \\ &= \frac{EA\pi^3}{4L^3} \sum_{m=1}^{\infty} \sum_{n=1}^{\infty} y_m(t) y_n(t) mn \left[ (m+n) \sin \frac{(m+n)\pi x}{L} \right. \\ &\quad \left. + (m-n) \sin \frac{(m-n)\pi x}{L} \right]. \end{aligned} \tag{8.55}$$

Under the assumptions of fixed boundary conditions and no dissipation, the longitudinal displacement becomes

$$\xi(x,t) = \sum_{k=1}^{\infty} \xi_k(t) \sin \frac{k\pi x}{L} = \sum_{k=1}^{\infty} \xi_k(x,t). \tag{8.56}$$

The component $\xi_k(x,t)$ will be excited under the condition that the projection of $f_{\mathrm{TL}}$ on this component is not equal to zero. This is checked by calculating the scalar product:

$$f_{\mathrm{TL},k}(t) = \int_0^L f_{\mathrm{TL}}(x,t) \sin \frac{k\pi x}{L} dx. \tag{8.57}$$

The calculation (8.57) then shows that the only cases where $f_{\mathrm{TL},k} \neq 0$ are obtained under the following conditions:

$$m + n = k \quad \text{or} \quad |m - n| = k. \tag{8.58}$$

In the first case (or "+" case), we have

$$f^{+}_{\mathrm{TL},k}(t) = -\frac{EA\pi^3}{8L^2} \sum_{n=1}^{k-1} y_{k-n}(t) y_n(t) k(k-n)n, \tag{8.59}$$

and, in the second case (or "−" case):

$$f^{-}_{\mathrm{TL},k}(t) = -\frac{EA\pi^3}{4L^2} \sum_{n=1}^{\infty} y_{k+n}(t) y_n(t) k(k+n)n. \tag{8.60}$$

From a spectral point of view, the previous equations yield the conditions that govern the occurrence of frequencies due to longitudinal vibrations of the string. For harmonic spectra, it can be checked (8.59) and (8.60) that these conditions are written:

$$\begin{cases} \text{for } f^{+}_{\mathrm{TL},k}(t) \ : \ f_n + f_{k-n} = f_k \ \text{ and } \ f_n - f_{k-n} = f_{|2n-k|}, \\ \text{for } f^{-}_{\mathrm{TL},k}(t) \ : \ f_n + f_{k+n} = f_{2n+k} \ \text{ and } \ f_n - f_{k+n} = f_k. \end{cases} \tag{8.61}$$

Such selection rules were applied successfully by Valette and Watzky to account for the generation of longitudinal modes in harpsichord strings [73]. They also account for "phantom partials" observable in piano sounds [17]. In the case of the piano, Bank and Sujbert made systematic measurements of real sounds that helped in enlarging the validity of relations (8.61) to the case of slightly inharmonic signals [7].

### 8.3.4 *Exact Geometrical Model of Piano Strings with Intrinsic Stiffness*

The general considerations on the nonlinear properties of strings presented in Sects. 8.3.1–8.3.3 above were based on simplified models of geometric nonlinearity and, in particular, on first-order approximations of the nonlinear terms in the wave equations. However, it has recently been demonstrated that the numerical simulations based on these approximate models can lead to errors, and even to instabilities [12]. In addition, as mentioned in several chapters of this book, and, particularly, in Chap. 3, the intrinsic stiffness of strings is an essential property, with significant audible consequences for the piano [26]. As shown below, the association of nonlinearity and stiffness is necessary in order to obtain a realistic model of piano

string. It is also preferable to use a geometrically exact model of string vibrations. Such a model has recently been developed by Chabassier et al., who write the nonlinear piano string's equations [13]:

$$\begin{cases} \rho A \dfrac{\partial^2 u_s}{\partial t^2} - \dfrac{\partial}{\partial x}\left[ EA \dfrac{\partial u_s}{\partial x} - \dfrac{(EA - T_0)\dfrac{\partial u_s}{\partial x}}{\sqrt{\left(\dfrac{\partial u_s}{\partial x}\right)^2 + \left(1 + \dfrac{\partial v_s}{\partial x}\right)^2}} \right] + AG\kappa \dfrac{\partial}{\partial x}\left(\varphi_s - \dfrac{\partial u_s}{\partial x}\right) = S, \\ \rho A \dfrac{\partial^2 v_s}{\partial t^2} - \dfrac{\partial}{\partial x}\left[ EA \dfrac{\partial v_s}{\partial x} - \dfrac{(EA - T_0)\left(1 + \dfrac{\partial v_s}{\partial x}\right)}{\sqrt{\left(\dfrac{\partial u_s}{\partial x}\right)^2 + \left(1 + \dfrac{\partial v_s}{\partial x}\right)^2}} \right] = 0, \\ \rho I \dfrac{\partial^2 \varphi_s}{\partial t^2} - EI \dfrac{\partial^2 \varphi_s}{\partial x^2} + AG\kappa \left(\varphi_s - \dfrac{\partial u_s}{\partial x}\right) = 0. \end{cases} \tag{8.62}$$

In this system, $u_s$ is the transverse component of the string's displacement, $v_s$ is the longitudinal component, and $\varphi_s$ is the angle of rotation of the cross-sections (see Fig. 8.8).[4] $\rho$ is the density of the string. For an homogeneous steel string, the string density is equal to the density of the material $\rho_c$, where the index "c" means "core." Similarly, the area of the cross-section is $A = A_c$. For the wrapped bass strings, where the wrapping (usually in copper) is aimed at increasing the mass without altering too much the stiffness, the density can be written $\rho = \rho_c F$, where $F$ is the wrapping factor defined as [15] :

$$F = 1 + \frac{\rho_w A_w}{\rho_c A_c}. \tag{8.63}$$

[4]Strictly speaking, the model should contain an additional horizontal component. In fact, it is observed experimentally that the polarization of most piano strings changes with time. It is often almost vertical during the initial transient, due to the action of the hammer, and is then evolving progressively towards a horizontal motion, even for small amplitudes. It can be demonstrated mathematically that such a polarization change can only occur if some asymmetry exists in the system that allows a transfer of energy from one component to the other. If the string is assumed to be homogeneous and perfectly rectilinear, with ideal boundary conditions (assuming a vertical motion of the bridge, for example), then the string will keep the initial polarization induced by the hammer during its motion. In [13], the authors made such assumptions, with a vertical initial motion of the hammer, and this is the reason why only one transverse component of the string is considered here. Revisiting the bridge model would be necessary for allowing a horizontal component.

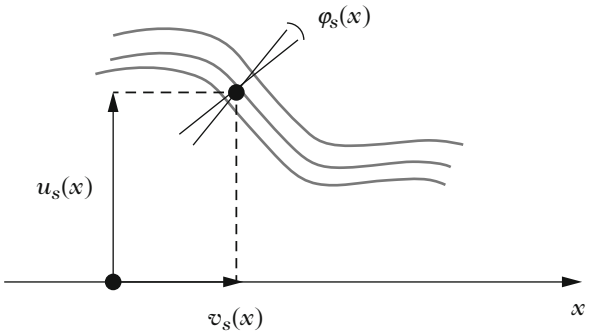


**Fig. 8.8** Variables for the nonlinear planar motion of a stiff string: $u_s$ is the transverse component, $v_s$ is the longitudinal component, and $\varphi$ is the angle of rotation of the cross-section due to shear stress

In this expression, $A_w$ is the cross-sectional area and $\rho_w$ the density of the wrapping. The other parameters (Young's modulus $E$, tension at rest $T_0$, torsional modulus $G$, and shear coefficient $\kappa$) are related to the core. The stiffness model in Eq. (8.62) is a Timoshenko model. Its main property follows from the coupling between transverse and shear waves. Accounting for shear yields accurate estimation of the string's eigenfrequencies in the audible range. In addition, the Timoshenko model has desired mathematical properties for the simulations. As shown in Chap. 3, for example, the transverse velocity in a Timoshenko beam tends to an asymptotic value as the frequency increases, whereas it tends to infinity for an Euler–Bernoulli beam, which is unsatisfactory from both a physical and numerical point of view. The source term $S$ in (8.62) accounts for the action of the hammer. To be complete, the model must also contain damping terms, which are not written here for the sake of simplicity.

The motion of the string imparts transverse and longitudinal forces at the bridge (see Fig. 8.9). These forces are transmitted to the soundboard, as a result of the particular geometry of the system and, also probably, because of the complex motion of the bridge. This motion is left aside here, since it is still not completely understood today, and subjected to some controversy. Considering then the angle between the string and the horizontal plane, only, then the two components of the string force at the bridge (in $x = L$) can be written as:

$$F_b(t) = \cos\alpha \left[ EA\,\partial_x u_s + AG\kappa\big(\partial_x u_s - \varphi_s\big) - (EA - T_0)\frac{\partial_x u_s}{\sqrt{(\partial_x u_s)^2 + (1 + \partial_x v_s)^2}} \right](x = L, t)$$
$$+ \sin\alpha \left[ EA\,\partial_x v_s + (EA - T_0)\big(1 - \frac{1 + \partial_x v_s}{\sqrt{(\partial_x u_s)^2 + (1 + \partial_x v_s)^2}}\big) \right](x = L, t). \tag{8.64}$$

The nonlinear string force (8.64) is the exact expression to be used in simulations. However, it is interesting to examine lower-order expansions of this force for the purpose of a physical interpretation. We get

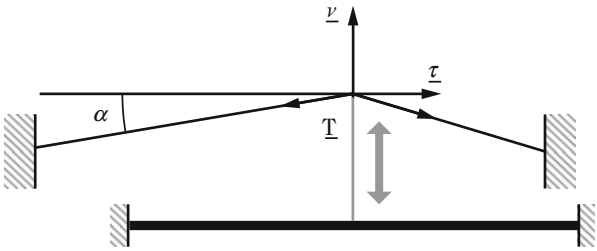


**Fig. 8.9** String–soundboard coupling at the bridge, allowing the transmission of the transverse and longitudinal components of the string force

$$
\begin{aligned}
F_b(t) \approx \cos(\alpha) \Big[ & T_0\, \partial_x u_s + AG\kappa \big(\partial_x u_s - \varphi_c\big) \\
& + (EA - T_0) \partial_x u_s\, \partial_x v_s + (EA - T_0) \frac{(\partial_x u_s)^3}{2} \Big] (x = L, t) \\
& + \sin(\alpha) \left[ EA\, \partial_x v_s + (EA - T_0) \frac{(\partial_x u_s)^2}{2} \right] (x = L, t).
\end{aligned}
\tag{8.65}
$$

In (8.65), the term $(T_0 + AG\kappa)\partial_x u_s$ contains the linear components of higher magnitude. The following term refers to the shear wave, and has no effect on the piano sound since the corresponding spectrum is beyond the audible range. The term $(EA - T_0)\partial_x u_s\, \partial_x v_s$ shows the possible existence of spectral combinations between transverse and longitudinal modes. The term $(EA - T_0)\frac{(\partial_x u_s)^3}{2}$ accounts for cubic transverse nonlinearities. The term $EA\, \partial_x v_s$ accounts for the longitudinal components. Finally, the term $(EA - T_0)\frac{(\partial_x u_s)^2}{2}$ accounts for quadratic transverse nonlinearities. This last term is comparable to the one discussed in Sect. 8.3.3. This shows that the nonlinear expression of the force transmitted from string to soundboard accounts for the richness of piano sounds. In addition to transverse and longitudinal partials, which are easily seen on real piano spectra because of their relative high amplitudes, the spectral analysis of piano tones show many other peaks due to combinations of order 2 or 3 between all components. These combinations are nothing but the famous *phantom* partials, as designated in the literature [16].

The experimental identification of these phenomena is shown in Fig. 8.10. The transverse partials are the peaks of highest amplitude: they are designated by a single number. On the top figure, the spectral peaks of smaller amplitude located between the transverse partials are the result of quadratic nonlinearity: they are designated by the sum of two numbers. The frequency of the phantom partial "14+16," for example, is equal to the exact sum (within 1 Hz, which corresponds to the accuracy of the spectral analysis) of the respective frequencies of partials 14 and 16. Here, one can realize the importance of inharmonicity: with a perfect harmonic transverse series of partials, it would be impossible to detect the phantom partials. In the previous example, the phantom partial "14+16" would be then superimposed to the 30th harmonic component. As shown in Chap. 3, the inharmonicity (due to stiffness)

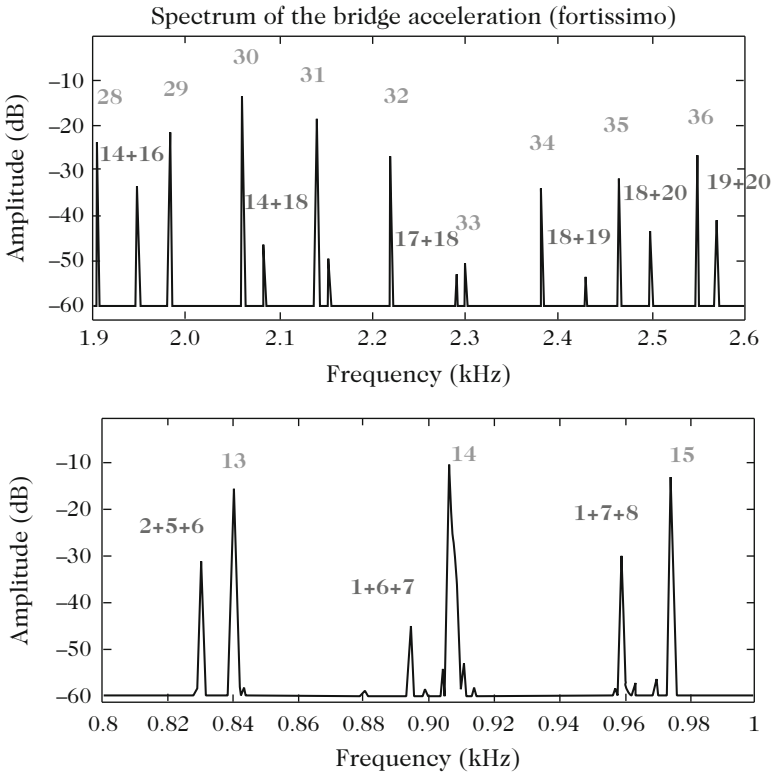


**Fig. 8.10** Experimental identification of phantom partials due to quadratic (*top*) and cubic (*bottom*) nonlinearities in the bridge acceleration spectrum, at the attachment point of string C2 (fundamental $f = 65.4$ Hz) of an upright piano

increases as the square of the partial's rank. Thus, the 30th transverse partial has a frequency higher than the "14 + 16" phantom partial. Similar comments can be made for the bottom figure where the added phantom partials are due to cubic nonlinearity. As a consequence, their frequencies are the combinations of three different frequencies of transverse partials. Zooming on other parts of the spectrum (not shown here) would illustrate other types of combinations, where the frequencies of some phantom partials are the sum of transverse and longitudinal frequencies, for example.

The issue of frequency combinations and added partials due to geometric nonlinearity will be addressed again in Sect. 8.5 devoted to gongs and cymbals. The mechanisms of instability at the origin of these new frequencies and the conditions for their existence will be analyzed and discussed.

## 8.4 Nonlinearities in Wind Instruments Resonators

In the previous chapters, the propagation of sound in wind instruments was based on the wave equation (cf. Chap. 1) obtained from basic equations (conservation equations, adiabatic behavior of ideal gas), through linearization of acoustic quantities with regard to the fluid at rest, considered as a reference state. The so-called small perturbations hypothesis is no longer justified in situations with high levels of sound, as the acoustic pressure amplitude inside the tube can reach 1–10 % of the atmospheric pressure. In this case, the phenomena must be analyzed with nonlinear propagation equations. The purpose of this section is to present basic tools of weakly nonlinear acoustics applied to one-dimensional waveguides (case without source, fluid at rest), and to discuss one particularly impressive wave distortion phenomenon, the so-called brassy sounds, observed in brass instruments.[5] In addition to brassy sounds, the nonlinear localized dissipation found in side-hole instruments, will also be examined (Sect. 8.4.5).

### *8.4.1 Nonlinear Propagation*

#### 8.4.1.1 From Basic Equations to the Weakly Nonlinear Wave Equation

A criterion for evaluating the relevance of the linear approximation consists in checking that the (dimensionless) acoustic Mach number $M = v_a/c$ is small compared to unity ($v_a$ is the amplitude of the acoustic velocity, whereas $c$ is the speed of sound). Reciprocally, in the case of very intense sound level (with $M$ of the order of unity), which corresponds to highly nonlinear acoustics, the basic equations cannot be linearized anymore! In fact, even for small acoustic Mach number, it is possible to observe pronounced nonlinear distortion phenomena. These effects are negligible on a small spatial scale: for distances small compared to the wavelength, it is possible to assume $p = \rho c v$ (as for a simple traveling wave). However, these effects are cumulative in space, for distances corresponding to a significant number of wavelengths, and can then generate highly distorted waves, and even shock waves.[6] This area of study is referred to as "weakly nonlinear" acoustics.

Nonlinear Equation of Wave Propagation

In the simple case of 1D linear acoustics, the propagation equation can be put in the form of two traveling wave equations of order 1, without a source: $\partial p/\partial t \pm$

[5] For a more detailed study of fundamental nonlinear acoustics, the reader may refer, for example, to the following authors: [18, 34, 54, 57].

[6] A shock wave is a pressure field which has an abrupt, and almost discontinuous, transition.

$c\partial p/\partial x = 0$. To generalize this, one can start from the basic equations of mass conservation (1.107) and momentum conservation (1.101), so that the quadratic nonlinear terms appear

$$\frac{\partial \rho}{\partial t} + \frac{\partial(\rho v)}{\partial x} = 0 \ ; \rho\left(\frac{\partial v}{\partial t} + v\frac{\partial v}{\partial x}\right) = -\frac{\partial P}{\partial x}. \tag{8.66}$$

Here, the initial symbols of the basic acoustic equations are used (i.e., before linearization), where $\rho$ and $P$ are the density and total pressure, respectively. Under the assumption of adiabaticity, $\rho$ depends only on $P$, or vice versa (adiabaticity is defined in Chap. 1). In addition, the velocity $v$ is also assumed to be a function of pressure $P$. The following system of equations is derived

$$\begin{aligned} \frac{d\rho}{dP}\frac{\partial P}{\partial t} + \frac{d(\rho v)}{dP}\frac{\partial P}{\partial x} &= 0 \\ \rho\frac{dv}{dP}\frac{\partial P}{\partial t} + \left(\rho v\frac{dv}{dP} + 1\right)\frac{\partial P}{\partial x} &= 0. \end{aligned} \tag{8.67}$$

It has nontrivial solutions for $\partial P/\partial t$ and $\partial P/\partial x$ if the determinant associated with the system of these two equations is equal to zero, which gives

$$\frac{d\rho}{dP}\left(\rho v\frac{dv}{dP} + 1\right) - \frac{d(\rho v)}{dP}\rho\frac{dv}{dP} = 0 \ \text{, equivalent to } \frac{d\rho}{dP} = \rho^2\left(\frac{dv}{dP}\right)^2.$$

By definition, we have $c^2 = dP/d\rho$. This leads to two solutions: "outgoing" and "incoming" traveling waves, respectively, corresponding to $dP/dv = \pm\rho c$. In the particular case of the outgoing wave, using the first Eq. (8.67), the so-called nonlinear propagation equation of the simple wave [24] is obtained

$$\frac{\partial P}{\partial t} + (c + v)\frac{\partial P}{\partial x} = 0. \tag{8.68}$$

This equation, obtained without any approximation, is nonlinear. Now, the speed of sound has to be expressed. In Chap. 5 the following nonlinear state equation was established in the case of an ideal adiabatic fluid:

$$\frac{P}{P_0} = \left(\frac{\rho}{\rho_0}\right)^\gamma \ \text{ from which } \ c^2 = \frac{dP}{d\rho} = \gamma\frac{P_0}{\rho_0}\left(\frac{\rho}{\rho_0}\right)^{\gamma-1}.$$

Weakly Nonlinear Acoustics Assumption

Under the assumption of weakly nonlinear acoustics, an approximate version of the simple wave equation (8.68) is now derived. Restricting the study to quadratic terms,

it is sufficient to write a first-order approximation of the speed of sound as a function of density, which gives

$$c \simeq c_0 \left[1 + \frac{\gamma - 1}{2} \frac{\rho'}{\rho_0}\right] \quad \text{with } c_0^2 = \gamma \frac{P_0}{\rho_0}. \tag{8.69}$$

$\rho'$ is still the acoustic density: $\rho = \rho_0 + \rho'$. The pressure is also assumed small, using the following notation (see Chap. 1): $P = P_0 + p$. Thus, we have $p/P_0 = \gamma \rho'/\rho_0$. Again to the first order, we have $p = \rho_0 c_0 v$, which yields

$$c_0 \frac{\rho'}{\rho_0} = \frac{c_0}{\gamma} \frac{p}{P_0} = v, \text{ and then } c = c_0 + \frac{\gamma - 1}{2} v. \tag{8.70}$$

Finally, the nonlinear equation (8.68) is approximated as follows:

$$\frac{\partial p}{\partial t} + (c + v) \frac{\partial p}{\partial x} = \frac{\partial p}{\partial t} + \left[c_0 + \frac{\gamma + 1}{2} v\right] \frac{\partial p}{\partial x} = 0. \tag{8.71}$$

This wave equation also remains valid, if we replace $p$ by $v$ or $\rho'$. In summary, Eqs. (8.68) and (8.70) account for the causes of nonlinearity present in both the conservation and the state equations:

- the convection effects (due to flow velocity). For a fixed observer, each point of the wave, instead of moving at the same speed $c_0$ is moving in fact at speed $c + v$, so faster at the maxima of the acoustic velocity, and slower at the minima.
- variations in the sound pressure induce compression and expansion zones that increase and decrease with temperature, respectively. Since the local speed of sound $c$ depends on temperature, it is also a function of the acoustic velocity.

As discussed in Sect. 8.4.2, the nonlinear traveling wave equation obtained above can be solved accurately by the method of Riemann invariants, also called the method of characteristics. The wave equation can also be established in the general case (non-traveling wave case), but it cannot be solved accurately. Notice that losses were not considered in the previous developments. If losses are taken into account, approximate methods, using perturbation calculus, should be used. Burgers equation mentioned in the following Sect. 8.4.1.2 is the result of such methods.

#### 8.4.1.2 Burgers Equation

The exact solution of nonlinear acoustics including losses is not possible. An approximate way to tackle the problem is to use a perturbation method: the method of "multiple scales".[7] This method is based on the presence in the equation of a

[7] This method is detailed in Sect. 8.5 devoted to nonlinear vibrations of gongs and cymbals.

small parameter, compared to unity: in our case, the selected parameter is the Mach number defined in the vicinity of the acoustic source of the system. This number serves as a basis for the definition of different scales: a short spatial scale (or "fast" scale) that describes the wave propagation locally, and a long spatial scale (or "slow" scale) that represents the cumulative effects of nonlinear distortion and losses. After some mathematical operations, that will not be detailed here, the weakly nonlinear lossless wave equation (8.71) is approximated by the following so-called Burgers equation:

$$\frac{\partial q}{\partial \sigma} - q\frac{\partial q}{\partial \theta} = 0, \tag{8.72}$$

where $q$ is a dimensionless velocity, $\sigma$ is a long spatial quantity, and $\theta$ is a dimensionless delayed time quantity. For more details, the reader may consult [57] or [19]. If the Burgers equation above is valid for the speed of sound, it is also applicable to other acoustic quantities, such as density and pressure. Equation (8.72) has an exact solution for $\sigma < 1$. For the particular case of a sine wave at the input ($\sigma = 0$), Fubini has obtained the solution [25]:

$$q(\sigma, \theta) = 2\sum_{n=1}^{\infty} \frac{J_n(n\sigma)}{n\sigma} \sin(n\theta), \tag{8.73}$$

where $J_n$ is the Bessel function of order $n$. "Generalized" Burgers equations exist, that take additional physical phenomena into account. As a consequence, the nonlinear differential equation that follows has two terms on the right-hand side, the first corresponding to volume visco-thermal phenomena, and the second to visco-thermal losses localized near the walls[8]:

$$\frac{\partial q}{\partial \sigma} - q\frac{\partial q}{\partial \theta} = A\frac{\partial^2 q}{\partial \theta^2} + B\frac{\partial^{1/2} q}{\partial \theta^{1/2}}, \tag{8.74}$$

where A and B are constants depending on the thermodynamic constants of both the gas and geometric characteristics of the system under study. In practice, the volume losses term can be ignored almost everywhere (i.e., outside the shock zone[9]) in the "sound pipes" application. Nevertheless, it is possible to separate and measure the relative influence of all these effects, using dimensional analysis (see, for example, [44]).

[8]So far, the volume visco-thermal losses, proportional to $\omega^2$, were ignored because in a wind instrument they are very low compared to losses in the boundary layers, proportional to $\sqrt{\omega}$. However, volume losses are essential in free space. Equation (8.74) including only the volume loss term ($B = 0$) is the equation called "Burgers equation," referring to the similar nonlinear equation used by the Dutch physicist J.M. Burgers in his work on turbulence.

[9]The shock zone is the zone where sudden changes of pressure, acoustic velocity, and temperature may occur.

### 8.4.2 Nonlinear Distortion and Shock Waves, Method of Characteristics

The nonlinearity of Burgers equation allows us to understand the origin of abrupt changes in pressure, which will be assumed to be discontinuous to a first approximation, although strictly discontinuous phenomena do not exist in real life.

To build simple analytical solutions to this equation, the mathematical method known as the method of characteristics (or *Riemann invariants method*) is used (however, this method will not be detailed here [34]). In what follows, we restrict ourselves to a qualitative description. Notice that this method is applicable to other discontinuous phenomena such as road traffic or the formation of tidal bores.

Losses are ignored in a first step. From the weakly nonlinear equation (8.71), it is derived that the velocity of a signal point propagating along the $x$-axis for a fixed observer is $c = c_0 + \frac{1}{2}(\gamma + 1)v$. The maximum of the acoustic wave propagates faster than the minimum. The wave becomes distorted during the propagation (see Fig. 8.11). Under the assumption of weak nonlinearity, any signal (plane wave) is necessarily transformed into a shock wave, even if the sound level at the source is low, as long as the dissipative phenomena are not taken into account, as is done here. The higher the amplitude of the wave at the origin, the faster the wave is distorted, and the shorter is the distance $x_c$ where the shock wave grows [54]. Using the method of characteristics, one can show that this distance is written:

$$x_c = \frac{2\gamma P_0 c_0}{(\gamma + 1)\,[\mathrm{d}p/\mathrm{d}t]_{\max}} \text{ where } [\mathrm{d}p/\mathrm{d}t]_{\max} \text{ at } x = 0. \tag{8.75}$$

From (8.75), it turns out that $x_c$ also depends on the shape of the signal, through the term $[\mathrm{d}p/\mathrm{d}t]_{\max}$. Thus, for an initially sinusoidal signal, $x_c$ is a decreasing function of frequency.

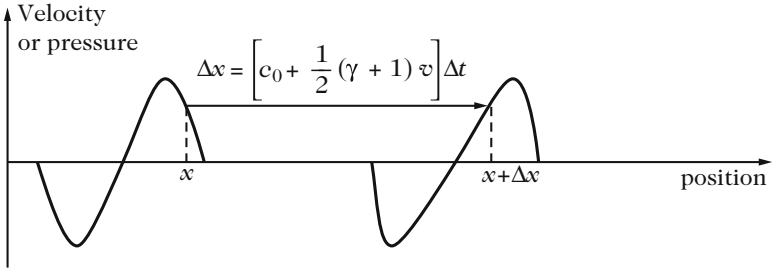


**Fig. 8.11** Wave distortion: evolution of a sinusoidal signal for a traveling plane wave (pressure or velocity) governed by the weakly nonlinear equation. Each point of the waveform travels with a given characteristic velocity that depends of the amplitude, which distorts the signal

Equation (8.68), with (8.70), implies that the acoustic velocity $v$ is constant over time ($dv/dt = 0$) along some lines (the so-called characteristics) of slope $c = c_0 + \frac{1}{2}(\gamma + 1)v$ in the $(x, t)$-plane. The method of characteristics illustrates the "cumulative" effect of the nonlinear distortion during wave propagation. The intersection of two characteristics in this plane corresponds to two possible values of sound pressure at the same point simultaneously: this corresponds to the formation of a shock wave. The first intersection yields an estimation for the shaping distance of the shock wave $x_c$. Beyond this point, the method of characteristics implies the existence of multivalued solutions, which is non-physical! It becomes then necessary to introduce a new condition to describe the shock. This condition is given by writing the conservation of mass across the shock wave, the so-called law of equal areas. It follows that the structure of the wave has a "sawtooth" shape, with a decreasing amplitude in the subsequent propagation. This wave is also called the "N-wave" (see, e.g., [54]).

The distortion of an initially sinusoidal wave is shown in the frequency domain as an energy transfer from the fundamental component of the signal to higher order harmonics [this is illustrated quantitatively by the Fubini equations (8.73)].

### *8.4.3 Competition Between Nonlinear Effects and Dissipation*

In the absence of losses, the model systematically predicts wave distortion and N-wave formation. The amplitude of this wave decreases, regardless of the intensity of the source signal (even if it is very low), and whatever the shape of the signal, as long as the wave propagates far enough! This is in contradiction with experiments showing that the initial amplitude of the source signal influences the nature of the produced sound. The model is therefore incomplete.

Taking the losses into account helps in obtaining a model which is closer to reality. The goal here is to a priori estimate the order of magnitude of competing phenomena: nonlinear effects and visco-thermal losses. As a consequence, losses may damp the signal before it has time to distort. In this case, the context of linear acoustics is sufficient to model the phenomena. For strong nonlinear phenomena, a possibility exists when the amplitude of the $N$-wave becomes low enough so that the dissipative effects are dominant. Since the visco-thermal losses at walls are an increasing function of frequency, the $N$-wave is damped and deformed over time to tend ultimately to a sinusoidal signal of very low amplitude. Notice that, during the formation of the shock wave, both the volume visco-thermal losses (usually ignored in the pipe) and visco-thermal losses in the boundary layer describe the shock wave shape correctly. In practice, the angles of the shock wave are "rounded" by dissipation.

### 8.4.4 *Shock Waves and Brassy Sounds*

The sound levels inside wind instruments can be very high (about 130–170 dB), and only a small part of the acoustic energy is transmitted to the external air. One way to a priori notice the presence, or the absence, of nonlinear phenomena, consists in estimating the distance of shock formation from the source signal. This procedure has been used for pressure signals measured inside a trombone mouthpiece [35]. The measured distance is of the order of magnitude of several meters, which suggests the presence of spectacular nonlinear effects in the instrument (recall that the length of the cylindrical part of the trombone, the main slide, is between 2 and 3 m).

Internal acoustic pressures corresponding to a high F (F4—frequency 350 Hz) were measured at the input of a trombone slide and at the slide end, for various sound levels (see Fig. 8.12). It is observed that the input signal is slightly distorted for increasing amplitudes, and that a spectacular distortion is visible on the signal at the output of the slide. If a note is played at the sixth position (for a slide near its maximum length, 2.8 m, which enhances the cumulative effect of nonlinear propagation), the distortion is such that shock waves are visible. The resulting spectral enrichment of the higher harmonics is also found in the sound radiated by the instrument. These sounds with a specific tone color are often called "brassy sounds" by the players.

The question of the propagation in bells is not discussed here (see Chap. 7). Outside the instrument, the radiated sound looks like a series of pulses generated at the frequency of the played note (it is calculated in the model by deriving the flow rate at the output). These high frequencies are totally transmitted to the external air and do not return to the lips of the player. Thus, they are not involved in the

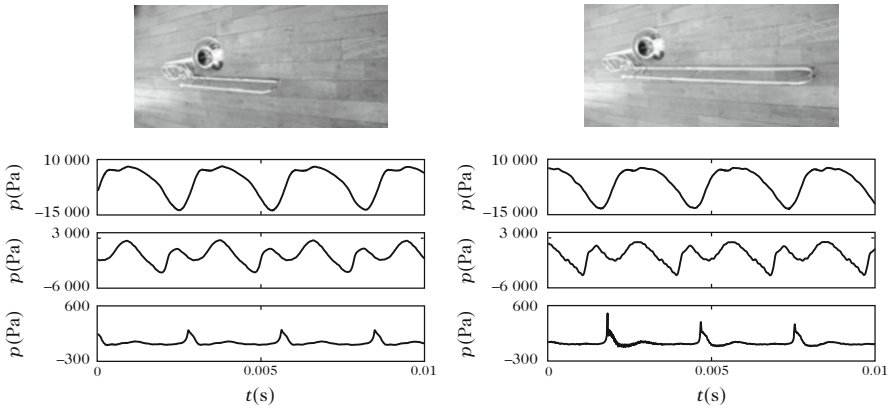


**Fig. 8.12** Shock waves in a trombone illustrated by pressure signals measured at the input of the instrument, at the slide output, and 20 cm outside the bell, respectively (*from top to bottom* on the figure). The note F4 (350 Hz) is played fortissimo in first (*left*) and in sixth position (*right*), the length of the cylindrical part being 1.80 and 2.80 m, respectively

self-sustained oscillations. This is an additional argument to justify the use of a linear propagation model (input impedance) for the analysis of sound production, which is the topic of the next chapter. In addition, this also justifies the following simplification currently used for synthesized sounds: in a first step, the synthesized sounds are obtained from a model of linear resonator, in a second step the sounds obtained at the input of the instrument propagate nonlinearly and radiate [47, 65, 74]. Such synthesized sounds simulate "brassy sounds" in a very realistic manner.

Only trombone brassy sounds were presented here, but in fact these "brassy sounds" are characteristics of all brass instruments, including those with predominantly conical bore. Nevertheless, the nonlinear distortion phenomenon is less pronounced in cones than in cylinders. We can probably see there an explanation for the distinction used by musicians between "bright brass" with a preponderant cylindrical bore (trumpet and trombone), and "soft brass" with a preponderant conical bore (cornet, flugelhorn, French horn, and tuba) (see Fig. 8.13) [50]. Another distinction between these types of instruments is due to the shape of the mouthpiece [28].

Woodwind instruments do not produce "brassy sounds," and it seems also that they are not subjected to, even small, nonlinear distortion effects [30]. However, nonlinear phenomena of a different nature can be seen, which are located at open holes, as it will be discussed in the next section.

**Fig. 8.13** Two examples of brass instrument families, each having one cylindrical bore instrument and another with a conical bore. *Left*: trumpet (*cylindrical*) and bugle (*cone*). *Right*: trombone (*cylindrical*) and low saxhorn (*cone*)

### 8.4.5 *Localized Nonlinear Dissipation*

When the particle velocity is high, jet separation phenomena at geometric singularities, like openings, may occur (see, for example, Chap. 10, Sect. 10.3.1.2). These phenomena, which are standard in fluid mechanics, occur less frequently in acoustics since they only appear for velocities larger than or equal to nearly 1 m/s, which corresponds to very intense sound levels.[10] However, these velocities correspond to a rather weak acoustic Mach number, which explains why these separation phenomena, when they occur, are generally more pronounced than the nonlinearity due to propagation. The phenomenon of jet separation may be of little consequence if it sticks quickly back to the wall. Otherwise, the interaction of the jet with the external fluid at rest generates vortices, because of shear effects. Part of the kinetic energy of the jet is absorbed by the vortices and further dissipated as heat by friction. This effect will be discussed in the next chapter where the output jet of a reed canal is examined. Finally, dissipation of acoustic energy exists, and the nonlinearity can be reasonably modeled as a nonlinear resistance.

#### 8.4.5.1 Simple Quasi-Static Model for the End of a Pipe

Consider the end of a tube, assuming zero impedance, in which a periodic flow has the form $v = v_0 \sin \omega t$. Assuming that a proportion of the kinetic energy is dissipated, the required pressure $p_s$ to maintain the flow is written:

$$p_s = c_d \frac{1}{2} \rho v \, |v| \, . \tag{8.76}$$

In fact there is no reason for the coefficient $c_d$ to be independent of speed. Atig et al. [5], in particular, have shown that this coefficient is larger when $v > 0$ (outgoing jet) that when $v < 0$ (incoming jet) and the value of this coefficient becomes larger as the radius of curvature at the pipe output decreases (see Fig. 8.14).

The same authors have shown elsewhere [4, 10] that considering either $c_d$ as a constant value, or two different values for the outgoing and incoming flows, respectively, has little influence on the oscillation of a clarinet, the relevant parameter being the average value of the coefficient. Therefore a model with one constant parameter, though very approximate, may lead to satisfactory results. In this case, we have

$$p_s = c_d \frac{1}{2} \rho v_0^2 \sin \omega t \, |\sin \omega t| = c_d \frac{1}{2} \rho v_0^2 \, \frac{8}{3\pi} \sin \omega t, \tag{8.77}$$

[10] For a pure traveling plane wave, a particle velocity of 1 m/s corresponds to a level of 400 Pa, or 146 dB SPL.

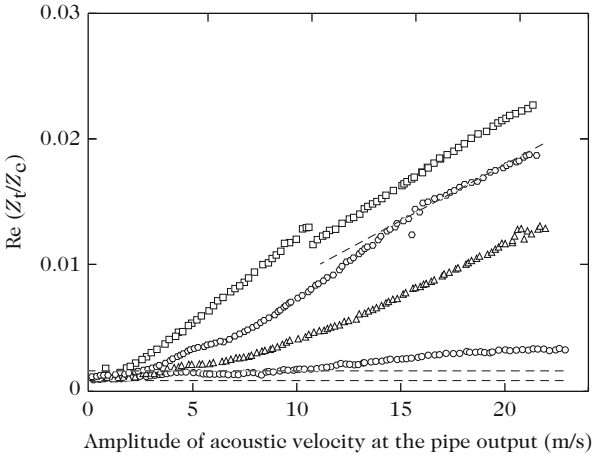


**Fig. 8.14** Real part of the normalized end impedance $Z_t/Z_c$ as a function of the velocity $v_0$ at the output of the pipe, for various radii of curvature $r$: *open circle* $r = 4$ mm; *triangle symbol*: $r = 1$ mm; *asterisk symbol*: $r = 0.3$ mm; *square symbol*: $r = 0.01$ mm. The inclined *straight dashed line* corresponds to the model of pressure losses for the outgoing jet with $c_d = 13/9$, and the two *horizontal dashed lines* correspond to the linear losses with and without screen, respectively. From [3]

if only the first term of the Fourier series is kept (first harmonic approximation). The power dissipated over a period is then:

$$P = \overline{p_s v} S = \frac{2c_d}{3\pi} \rho v_0^3 S. \tag{8.78}$$

Within the framework of the first harmonic approximation, assuming that the end impedance is real, it is found equal to:

$$Z_t = \frac{4c_d}{3\pi} M Z_c, \tag{8.79}$$

where $M = v_0/c$ is the acoustic Mach number. Experiments show that this simple model reflects the asymptotic behavior of nonlinear impedance fairly well (within the context of the first harmonic method). In practice, it is valid for high velocities (typically $v_0 > 10$ m/s, see Fig. 8.14). The definition of impedance in a nonlinear regime would deserve much more care, but if one satisfies with a perturbation approach (the linear speed is calculated, and injected in the "nonlinear" impedance expression), the validity of (8.79) can be assumed. The value of the coefficient $c_d$ is difficult to predict theoretically and it is easier to determine it experimentally.

#### 8.4.5.2 Side Hole

In the case of a side hole one can expect to see nonlinear resistances both in series and in parallel branches of the tube model (see Chap. 7). Dalmont et al. were able to highlight these resistances, however, they also have shown that the resistance in series could reasonably be neglected when the diameter of the side hole is significantly smaller than the diameter of the main guide [20]. Again here, the parameters are highly dependent on the radii of curvature at the junction and at the output of the hole. The use of nonlinear impedance in a calculation of input impedance, or of reflection impedance, can be done simply with perturbation methods.

The influence of high sound level (up to 10 kPa, or nearly 174 dB) on the self-sustained oscillations of a clarinet type instrument has been investigated ([4], see Chap. 9, Sect. 9.4.6) for a cylinder. It shows the importance of nonlinear losses at the end on sound pressure level. One can also show that losses in a side hole reduce the playing frequency, which is easily understood: if the, even real, impedance of a side hole, increases notably, it may eventually act as a closed end for the hole! The conventional calculation of playing frequency that ignores the losses and uses purely imaginary impedances, shows here an obvious limit. Debut et al. [21] proposed an approximate formula to account for this.

## 8.5 Geometric Nonlinearities in Gongs and Cymbals

Gongs and cymbals perfectly illustrate a number of fundamental properties of nonlinear systems: sensitivity to initial conditions, bifurcations, hysteresis, and routes to chaos. Geometric nonlinearities are also present in other instruments, such as the steelpan [45].

By striking an orchestral gong (also called a Chinese tam-tam, see Fig. 8.15) gently near its center with a mallet, one can clearly hear the excited modes and their extinction. The vibration is then adequately described by a linear model. If one hits harder, other frequencies appear, and a simple linear analysis does not account for them.

The vibration spectrum (and, consequently, that of the produced sound) can only be explained with the help of nonlinear theories that predict the existence of *combinations of resonances*. These combinations contribute to enrich the number of emitted frequencies considerably.

Finally, if one hits even stronger, this yields a continuous spectrum. In other words, the excited frequencies are no longer separable from one another. A detailed analysis performed on the obtained signals shows that *chaotic* oscillations are

**Fig. 8.15** Orchestral gong, or Chinese tam-tam. Courtesy © Rythmes et Sons

obtained (see Fig. 8.16).[11] The strict definition of this term will be specified later. Notice that, although the spectrum of the sound obtained at strong impact is continuous, it is not that of a random noise.

In this section, the nonlinear phenomena that are the origin of the specific sounds of those instruments are described. We show, in particular, that they are due to the *geometric nonlinearity* caused by large amplitude motion of the structure, when subjected to a strong impact. To facilitate the understanding, a simplified mathematical description of a subsystem composed of a small number of nonlinearly coupled oscillators will be conducted. Finally, the generalization to nonlinear continuous systems with a large number of degrees of freedom will be made. Spherical shells subjected to large amplitude oscillations will serve as an example of a structure for which an analytical description of such phenomena is possible.[12]

[11] The definition of chaos, as well as the method used for analyzing and quantifying such oscillations, will be presented throughout this chapter (see Sect. 8.6, in particular). Here, we can see some first properties of chaotic oscillations: irregularity in the time-domain, and a broadband spectrum where it is not possible to discriminate individual spectral peaks anymore. Sensitivity to initial conditions is another essential feature of chaotic oscillations, which will be discussed later in detail.

[12] An important part of the topics presented in this section are the results of new insights on the nonlinear vibrations of thin structures which were published during the last 15 years. See, in particular, the Ph.D. thesis by O. Thomas, and his joint work with colleagues [8, 11, 60, 61, 64, 68].

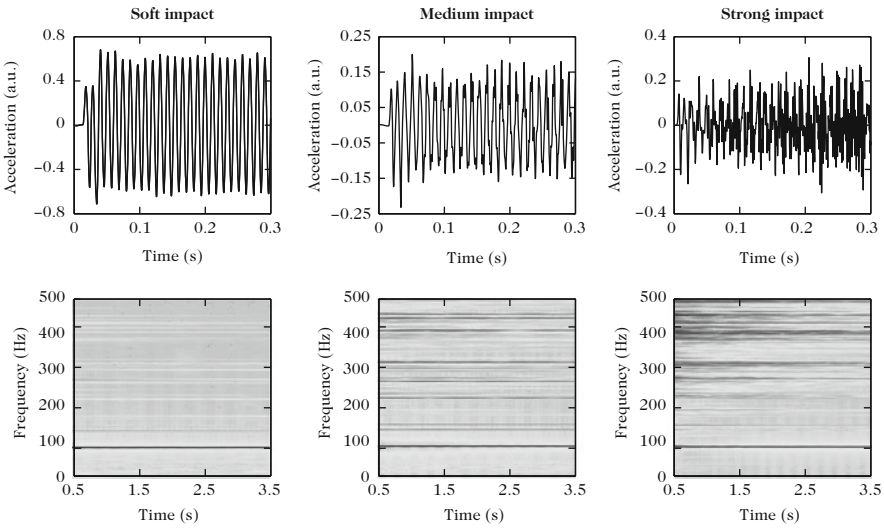


**Fig. 8.16** Vibration waveforms and spectra of a gong struck with increasing impact force. The three *upper figures* show the vibration signals delivered by an accelerometer glued to a gong excited near its center with a mallet. The three figures at the *bottom* show the corresponding spectrograms, which represent the spectral content of these signals over time. The *dark lines* corresponds to high level, the *light gray lines* to low level. For a "soft" impact, the vibration signal is almost sinusoidal, the spectrum shows an intense spectral line around 90 Hz, and only a few lines at higher frequencies, at a lower level. For a "medium" impact, the intensity of the 90 Hz component decreases, whereas the level of higher frequencies increases. Simultaneously, new components with a significant energy appear in the higher range of the spectrum. For a "strong" impact, the energy is still increasing in the high frequency range (between 200 and 500 Hz in the spectrogram), the spectrum becomes continuous, and it is no longer possible to separate the spectral lines. The waveform loses its periodic nature and becomes chaotic (see Sect. 8.6)

### *8.5.1 Sinusoidal Forced Excitation*

Impact clearly corresponds to the standard use for gongs and cymbals. However, it is difficult to analyze the phenomena, because of the large bandwidth of the excitation spectrum. For this reason, it is preferable to observe the phenomena experimentally with a forced sinusoidal excitation. This procedure has the advantage of presenting the main phenomena, and thus allowing easier modeling. Nevertheless, recall that, unlike the case of linear systems, one cannot conclude here that the oscillations obtained through normal impact are the superposition of the oscillations obtained by summing the results obtained for each frequency of the excitation spectrum, since the superposition principle is not anymore valid for nonlinear oscillations.

Figure 8.17 shows an example of experiments where the amplitude of the excitation force gradually increases at a given point of a gong. Similar experiments were conducted on cymbals. An excitation frequency close to one natural frequency of the structure is selected, in order to generate high amplitude. The vibration velocity is

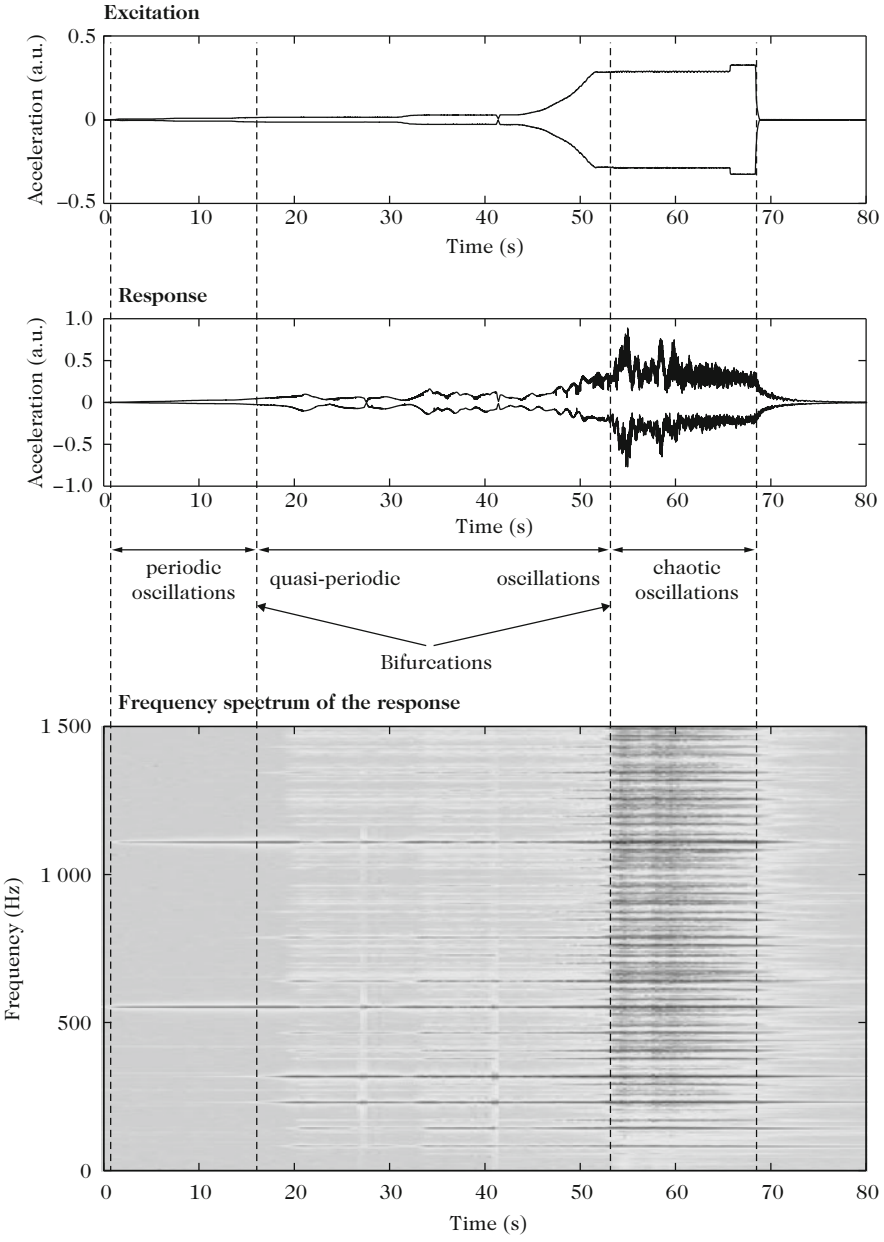


**Fig. 8.17** Forced sinusoidal excitation of a gong. (See [60] and Sect. 8.5.1 in the text for a detailed description of this experiment)

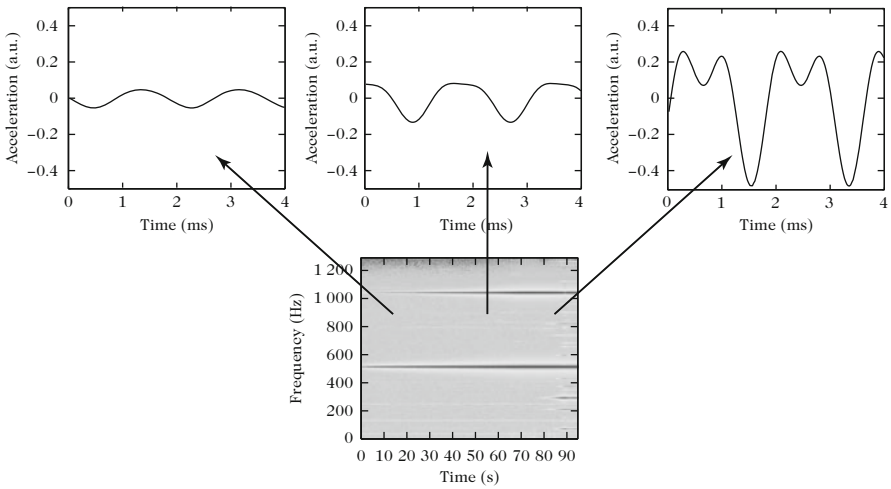


**Fig. 8.18** (*Top*) Vibration acceleration at a given point of the gong for increasing amplitude of the sinusoidal excitation force. (*Bottom*) Corresponding spectrogram. One can see an increasing distortion of the wave and an enrichment in harmonics in the spectrum over time. For reasons of clarity, the frequency scale on the spectrogram is intentionally reduced and does not show the higher harmonics $2\Omega$, $3\Omega$, $4\Omega$,... which are nonetheless present in the vibration spectrum

measured at a point on the structure with the help of a laser vibrometer. It is observed that the obtained waveform is, first, a sine wave. Some harmonics gradually appear as the amplitude of the excitation further increases (see Fig. 8.18). For a particular value of this amplitude (or *threshold*), additional frequencies suddenly appear in the spectrum and are inserted between the harmonics. A detailed examination of the values of these frequencies shows that they are algebraically related to the harmonic excitation. Moreover, they correspond to other eigenmodes of the structure than the one initially excited (see the next section). The emergence of these new frequencies is characteristic of what is called a *bifurcation*. Mathematically, we will see in the next sections that such a bifurcation corresponds to a loss of stability for the system, and that the stability domain depends on both the amplitude and frequency of the excitation.

When the amplitude of the exciting force continues to increase, there is a new threshold that causes a second bifurcation. For slightly damped systems, such as metallic percussion instruments, one reaches a chaotic regime on this second bifurcation. It can be seen in Fig. 8.17 that the vibration spectrum beyond this threshold is so dense that there it is almost continuous. When listening, the characteristic shimmering sound of a gong (or a cymbal) is easily recognized, although the instruments are excited with a single frequency.

### 8.5.2 Internal Resonances

To explain these phenomena, a brief return back to the linear case presented in Chap. 3 is necessary, where it was established that the vibrations of a conservative finite structure can be represented as a projection onto a eigenmodes basis. In what follows, we will see that the nonlinear behavior of gongs can be described with the help of their linear modal properties. As seen in Chap. 3, the linear motion of a structure, which is assumed to be non dissipative so far, can be written in the following generic form:

$$\mathscr{L}(\boldsymbol{\xi}) + \ddot{\boldsymbol{\xi}} = 0$$
$$+ \text{boundary conditions}, \tag{8.80}$$

where $\mathscr{L}$ is a *linear operator* involving the displacement field $\boldsymbol{\xi}$ of the structure and its spatial derivatives. Then, this motion can be decomposed on the basis of its own eigenmodes, each mode being characterized by an eigenfrequency and an associated eigenshape.

Thus, for a given material, geometry (thickness, curvature, size,...) and boundary conditions, the eigenfrequencies and eigenmodes of the structure are fully determined. If some algebraic relations exist between the eigenfrequencies, such as:

$$\sum_{i=1}^{L} m_i \omega_i = 0, \tag{8.81}$$

where $m_i$ is an integer (positive or negative), the structure is said to have *internal resonances*. Some relations of the following types, for example:

$$\omega_1 + \omega_2 = \omega_3 \quad \text{or} \quad 2\omega_3 - \omega_1 = \omega_5. \tag{8.82}$$

can be exhibited.

In the case of structures with a circular geometry, some other interesting properties are observed: one can discriminate between the *asymmetric* modes, and the *axisymmetric* modes which show a symmetry with regard to the revolution axis (see Fig. 8.19).

In fact, the *asymmetric* modes are grouped by pairs, whose mode shapes are identical, showing only a phase shift of $\pi/2p$, where $p$ is the number of nodal diameters. If the structure is perfectly homogeneous, the eigenfrequencies, denoted here, for example, $\omega_{n1}$ and $\omega_{n2}$, are theoretically identical. In practice, measurements show that these frequencies differ slightly, as a result of some unavoidable imperfections in the structure (which may include residual stresses), and because of the attachment system. For inhomogeneous structures (such as gongs), one can observe some important differences between both frequencies of a mode pair. An important subset of the relations (8.81) are those where:

$$m_k \omega_k = m_i \omega_i + m_j \omega_j \quad \text{with} \quad |m_i| + |m_j| = 2, \tag{8.83}$$

This type of internal resonance is of prime importance in the case of *quadratic nonlinearities*, which govern the physical behavior of gongs and cymbals.

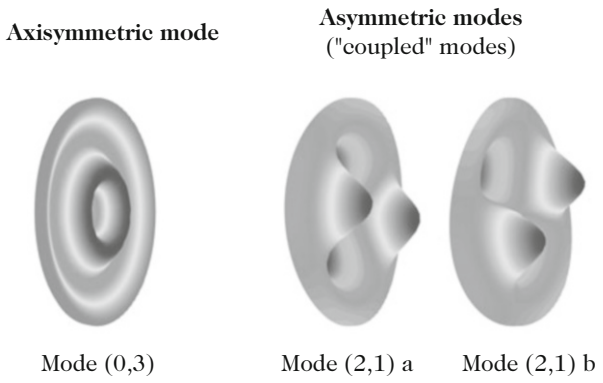


**Fig. 8.19** Examples of axisymmetrical modes and asymmetrical modes of a gong

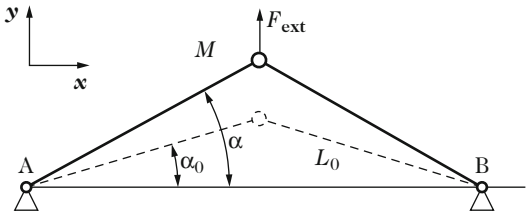


**Fig. 8.20** Set of two joint articulated bars illustrating an example of geometrical nonlinearity

### *8.5.3 Weakly Nonlinear Regime*

Structures such as gongs, cymbals, and thin spherical shells, show an asymmetry due to curvature. In fact, the transverse motion is easier in the direction of the hollow side than in the rounded one. This is an example of geometrical nonlinearity, which is comparable to the case of the interrupted pendulum seen in Sect. 8.1. Another qualitative interpretation of such a geometrical nonlinearity can be made for a simple system of two articulated rods oscillating around a position defined by an initial angle $\alpha_0$ that represents the curvature (see Fig. 8.20) [62].

Let $E$ be the Young's modulus of the rods, $A$ their cross-sectional area, and $L_0$ their length at rest. It can be shown that, under the action of a vertical force with amplitude $F$, the transverse displacement $y$ of the joining point of the rods is linked to the force by the relation:

$$F = 2EA \left\{ \frac{y}{L_0} \sin^2 \alpha_o + \frac{3}{2} \sin \alpha_0 \left( \frac{y}{L_0} \right)^2 + \frac{1}{2} \left( \frac{y}{L_0} \right)^3 \right\} . \tag{8.84}$$

Quadratic terms in $y^2$ are seen in Eq. (8.84). This equation also shows the presence of cubic terms: this result can be generalized to more complex curved structures,

something that we will admit here without proof.[13] Let us now return to the experiments of the gong excited at its center by a sinusoidal force of frequency $\Omega$ close to the eigenfrequency of one particular *axisymmetric* mode. As shown in Fig. 8.18, the increase of the excitation amplitude results in an asymmetry in the vibration waveform where the oscillations are more distorted for positive values of the acceleration than for negative values. It is an example of quadratic nonlinearity, which, in the spectral domain, is characterized by the presence of even harmonics ($2\Omega$, $4\Omega$,...).

Beyond the first bifurcation, a fine frequency analysis shows that the new frequencies arising in the spectrum are related to the driving frequency by the following combination rules, also called *combination of resonances*:

$$m_k\Omega = m_i\omega_i + m_j\omega_j \quad \text{with} \quad |m_i| + |m_j| = 2. \tag{8.85}$$

where $m_k$ is a positive integer, and $m_i$ and $m_j$ positive (or negative) integers. These combination rules are the result of both the internal resonances of the structure (particular relationships between eigenfrequencies) and quadratic nonlinearity. One practical consequence of the excitation of such frequencies is, for example, the possibility of exciting asymmetric modes with a shaker attached at the center of symmetry of the structure. This would never be possible in the linear regime (see Chap. 3) since this point corresponds to a node for asymmetric modes. A nonlinear coupling only can explain such a phenomenon. An experimental illustration of these resonances is described in Sect. 8.5.5.

### 8.5.4 Energy Transfer Through Combination of Resonances

To analyze the phenomena described above, a simple example of nonlinear quadratic coupling between two discrete oscillators will be used. The method of *multiple scales* is used for solving the problem [51]. The system under consideration is the following:

$$\begin{cases} \ddot{x}_1 + \omega_1^2 x_1 = \varepsilon\left[-\beta_{12}x_1x_2 - 2\mu_1 x_1\right], \\ \ddot{x}_2 + \omega_2^2 x_2 = \varepsilon\left[-\beta_{21}x_1^2 - 2\mu_2 x_2 + P\cos\Omega t\right]. \end{cases} \tag{8.86}$$

The variables $x_1$ and $x_2$ are the displacements of the oscillators. The frequencies $\omega_1$ and $\omega_2$ are the eigenfrequencies of each oscillator in its linear regime. In the absence of driving force, damping and nonlinearities, the system (8.86) reduces to the free oscillations of two independent linear oscillators. The right-hand sides of

[13] In this example, the terms in $y^2$ and $y^3$, respectively, are comparable as long as $\alpha_o$ is not supposed to be small. We will see later that the quadratic terms are predominant in thin shells.

the differential system (8.86) represent the perturbation terms with regard to this ideal linear case. The dimensionless quantity $\varepsilon \ll 1$ indicates that these terms are small. The quadratic nonlinear coupling is ensured by the terms $\beta_{12}x_1x_2$ and $\beta_{21}x_1^2$. It can be shown, and this will be assumed here, that these two terms are sufficient for guaranteeing the generality of quadratic coupling. In other words, it is not necessary to add a term in $x_2^2$, for instance, in the first equation, since an appropriate change of variables would yield a formulation similar to (8.86) (see a justification for this property in Sect. 8.7 devoted to nonlinear normal modes). As an example, a system with an internal resonance $\omega_2 = 2\omega_1 + \varepsilon\sigma_1$ is studied, where $\sigma_1$ is the parameter of *internal detuning*. The driving frequency $\Omega$ is chosen close to $\omega_2$ so that one can write $\Omega = \omega_2 + \varepsilon\sigma_2$ where $\sigma_2$ is the parameter of *external detuning*.

#### 8.5.4.1 Solution by the Method of Multiple Scales

In this section, we want to obtain the expressions of both amplitudes $a_1$ and $a_2$ of $x_1$ and $x_2$, respectively, as a function of frequency, or, equivalently, in terms of the external detuning parameter $\sigma_2$. We also want to determine the threshold values for which bifurcations occur. In the example presented here, this implies, in practice, to calculate the amplitude of the forcing term for which a subharmonic of order two of the driving frequency $\Omega$ just appears.

Principle and Main Steps of the Calculation

The example presented here is very rich, since it contains the essential concepts and methods used in the study of nonlinear oscillators. To assist the reader, we start by presenting a summary of the main steps of the calculation with their respective goals.

1. Definition of the time scales, and general form of the solution.
2. Solvability conditions. Elimination of the secular terms.
3. Autonomous system and fixed points.
4. Stability of the system.
5. Amplitudes and phases of the solution.

Time Scales and General Form of the Solution

The time scales are defined as:

$$T_j = \varepsilon^j t \quad \text{with} \quad j \geq 0, \tag{8.87}$$

and the solutions are expanded in increasing power of $\varepsilon$

$$\begin{cases} x_1(t) = x_{10}(T_0, T_1) + \varepsilon x_{11}(T_0, T_1) + O(\varepsilon^2), \\ x_2(t) = x_{20}(T_0, T_1) + \varepsilon x_{21}(T_0, T_1) + O(\varepsilon^2), \end{cases} \tag{8.88}$$

In what follows, the expansion is limited to the first order in $\varepsilon$. In (8.87), notice that the differentiation operators with respect to time are such that:

$$\begin{cases} \dfrac{\partial}{\partial t} = \dfrac{\partial}{\partial T_0} + \varepsilon \dfrac{\partial}{\partial T_1}, \\ \dfrac{\partial^2}{\partial t^2} = \dfrac{\partial^2}{\partial T_0^2} + 2\varepsilon \dfrac{\partial}{\partial T_0} \dfrac{\partial}{\partial T_1}. \end{cases} \tag{8.89}$$

From here, we use the notation $D_j = \frac{\partial}{\partial T_j}$. Inserting (8.89) in (8.86), and identifying the terms of identical power in $\varepsilon$, yields

- to order $\varepsilon^0 = 1$:

$$\begin{cases} D_0^2 x_{10} + \omega_1^2 x_{10} = 0, \\ D_0^2 x_{20} + \omega_2^2 x_{20} = 0, \end{cases} \tag{8.90}$$

- to order $\varepsilon$:

$$\begin{cases} D_0^2 x_{11} + \omega_1^2 x_{11} = -2D_0 D_1 x_{10} - \beta_{12} x_{10} x_{20} - 2\mu_1 D_0 x_{10}, \\ D_0^2 x_{21} + \omega_2^2 x_{21} = -2D_0 D_1 x_{20} - \beta_{21} x_{10}^2 - 2\mu_2 D_0 x_{20} + P \cos \Omega t. \end{cases} \tag{8.91}$$

The solutions of the system (8.90) are written in general form:

$$\begin{cases} x_{10}(t) = A_1(T_1) e^{j\omega_1 t} + A_1^\star(T_1) e^{-j\omega_1 t}, \\ x_{20}(t) = A_2(T_1) e^{j\omega_2 t} + A_2^\star(T_1) e^{-j\omega_2 t}, \end{cases} \tag{8.92}$$

where the exponent $(^\star)$ indicates the complex conjugate.

### Solvability Conditions

The complex quantities $A_1(T_1)$ and $A_2(T_1)$ are functions of $T_1 = \varepsilon t$, and are still unknown at this stage of the solving. To determine them, the expressions (8.92) are inserted in (8.91), and we derive the conditions for avoiding *secular terms* in the solution. This yields the so-called *solvability conditions* which are written here:

$$\begin{cases} -2j\omega_1\left(\dfrac{\partial A_1}{\partial T_1}+\mu_1 A_1\right)-\beta_{12}A_1^* A_2 e^{j\sigma_1 T_1}=0, \\ -2j\omega_2\left(\dfrac{\partial A_2}{\partial T_1}+\mu_2 A_2\right)-\beta_{21}A_1^2 e^{-j\sigma_1 T_1}+\dfrac{P}{2}e^{j\sigma_2 T_1}=0. \end{cases} \tag{8.93}$$

These Eqs. (8.93) are usually solved in the following polar form:

$$\begin{cases} A_1(T_1)=\dfrac{a_1}{2}e^{j\theta_1}, \\ A_2(T_1)=\dfrac{a_2}{2}e^{j\theta_2}, \end{cases} \tag{8.94}$$

where both the amplitudes $a_i$ and phases $\theta_i$ are functions of $T_1$. Substituting these expressions in (8.93), we get the dynamic system that governs the evolution of amplitudes and phases of the oscillators at the time scale $T_1$, corresponding to *slow* changes in the system. It is written here:

$$\begin{cases} \dfrac{\partial a_1}{\partial T_1}=-\mu_1 a_1-\dfrac{\beta_{12}a_1 a_2}{4\omega_1}\sin(\sigma_1 T_1+\theta_2-2\theta_1), \\ a_1\dfrac{\partial \theta_1}{\partial T_1}=\dfrac{\beta_{12}a_1 a_2}{4\omega_1}\cos(\sigma_1 T_1+\theta_2-2\theta_1), \\ \dfrac{\partial a_2}{\partial T_2}=-\mu_2 a_2+\dfrac{\beta_{21}a_1^2}{4\omega_2}\sin(\sigma_1 T_1+\theta_2-2\theta_1)+\dfrac{P}{2\omega_2}\sin(\sigma_2 T_1-\theta_2), \\ a_2\dfrac{\partial \theta_2}{\partial T_2}=\dfrac{\beta_{21}a_1^2}{4\omega_2}\cos(\sigma_1 T_1+\theta_2-2\theta_1)-\dfrac{P}{2\omega_2}\cos(\sigma_2 T_1-\theta_2). \end{cases} \tag{8.95}$$

### Autonomous System and Fixed Points

In order to determine the conditions for obtaining solutions to the nonlinear coupled system (8.86), it is necessary to express first Eq. (8.95) as an *autonomous system* or, equivalently, in the form $\dot{X}=F(X)$ where the time variable $T_1$ is no longer present in the right-hand side. In practice, this procedure is equivalent to using the variables $\gamma_1=\sigma_2 T_1-\theta_2$ and $\gamma_2=\sigma_1 T_1+\theta_2-2\theta_1$, which yields

$$\begin{cases} \dfrac{\partial a_1}{\partial T_1} = -\mu_1 a_1 - \dfrac{\beta_{12} a_1 a_2}{4\omega_1} \sin\gamma_2, \\ \dfrac{\partial \gamma_1}{\partial T_1} = \sigma_2 - \dfrac{\beta_{21} a_1^2}{4\omega_2 a_2} \cos\gamma_2 + \dfrac{P}{2\omega_2 a_2} \cos\gamma_1, \\ \dfrac{\partial a_2}{\partial T_2} = -\mu_2 a_2 + \dfrac{\beta_{21} a_1^2}{4\omega_2} \sin\gamma_2 + \dfrac{P}{2\omega_2} \sin\gamma_1, \\ \dfrac{\partial \gamma_2}{\partial T_2} = \sigma_1 - \dfrac{\beta_{12} a_2}{2\omega_1} \cos\gamma_2 + \dfrac{\beta_{21} a_1^2}{4\omega_2 a_2} \cos\gamma_2 - \dfrac{P}{2\omega_2 a_2} \cos\gamma_1. \end{cases} \tag{8.96}$$

The so-called *fixed points* are obtained by eliminating the time derivatives in (8.96). This corresponds to the stationary solutions of the system, i.e., those of interest in the case of a forced oscillations. We get

$$\begin{cases} a_1 \left( \mu_1 + \dfrac{\beta_{12} a_2}{4\omega_1} \sin\gamma_2 \right) = 0, \\ \sigma_2 - \dfrac{\beta_{21} a_1^2}{4\omega_2 a_2} \cos\gamma_2 + \dfrac{P}{2\omega_2 a_2} \cos\gamma_1 = 0, \\ -\mu_2 a_2 + \dfrac{\beta_{21} a_1^2}{4\omega_2} \sin\gamma_2 + \dfrac{P}{2\omega_2} \sin\gamma_1 = 0, \\ \sigma_1 + \dfrac{\beta_{21} a_1^2}{4\omega_2 a_2} \cos\gamma_2 - \dfrac{P}{2\omega_2 a_2} \cos\gamma_1 - \dfrac{\beta_{12} a_2}{2\omega_1} \cos\gamma_2 = 0. \end{cases} \tag{8.97}$$

**Note** Setting $a_1 = 0$ in (8.97) gives the expression for the amplitude $a_2$ of the second oscillator:

$$a_2 = \frac{P}{2\omega_2 \sqrt{\sigma_2^2 + \mu_2^2}}. \tag{8.98}$$

Recall that $\sigma_2$ is here the difference between the loading frequency and the oscillator's frequency, and that $\mu_2$ is the "fluid" damping parameter. Thus, the variation of amplitude with frequency of a forced linear oscillator is obtained (see Chap. 2).

### Stability of the Nonlinear Coupled System

Intuitively, the concept of instability can be represented by a physical system, slightly pushed aside from its equilibrium position, that continues to increasingly depart from equilibrium instead of returning back to it. In the case of gongs and cymbals, it is observed that, under a sufficient level of excitation, new frequencies

appear and, through a process of instability cascade (previously called nonlinear coupling), may lead to other components to form the richness of the sound.

From a mathematical point of view, the departures from equilibrium for a system of equations of several variables similar to (8.97) are calculated from the partial derivatives of each equation with respect to each variable. This yields what is called the *Jacobian matrix* or, more simply, the *Jacobian* of the system. Let $f_1, f_2, f_3, f_4$ be the four equations and $a_1, \gamma_1, a_2, \gamma_2$ the four variables of interest. The Jacobian is written:

$$\mathscr{J} = \begin{bmatrix} \frac{\partial f_1}{\partial a_1} & \frac{\partial f_1}{\partial \gamma_1} & \frac{\partial f_1}{\partial a_2} & \frac{\partial f_1}{\partial \gamma_2} \\ \frac{\partial f_2}{\partial a_1} & \frac{\partial f_2}{\partial \gamma_1} & \frac{\partial f_2}{\partial a_2} & \frac{\partial f_2}{\partial \gamma_2} \\ \frac{\partial f_3}{\partial a_1} & \frac{\partial f_3}{\partial \gamma_1} & \frac{\partial f_3}{\partial a_2} & \frac{\partial f_3}{\partial \gamma_2} \\ \frac{\partial f_4}{\partial a_1} & \frac{\partial f_4}{\partial \gamma_1} & \frac{\partial f_4}{\partial a_2} & \frac{\partial f_4}{\partial \gamma_2} \end{bmatrix}. \tag{8.99}$$

Each term of the Jacobian represents a small deviation from equilibrium. In order to calculate the stability of the equilibrium at point $a_1 = 0$, which corresponds to the conditions of appearance for oscillator 1, a standard method is used, where the eigenvalues $\lambda_i$ of $\mathscr{J}$ are calculated. These eigenvalues are the roots of the determinant $\mathscr{J} - \lambda\mathscr{I}$, where $\mathscr{I}$ is the identity matrix. The following four eigenvalues are found:

$$\begin{cases} \lambda_1 = -\mu_2 + j\sigma_2, & \lambda_2 = \quad -\mu_2 - j\sigma_2, \\ \lambda_3 = -\dfrac{\beta_{12} a_2}{4\omega_1} \sin\gamma_2 - \mu_2, & \lambda_4 = \quad \dfrac{\beta_{12} a_2}{2\omega_1} \sin\gamma_2. \end{cases} \tag{8.100}$$

The system will be *unstable* if the real part of at least one root is positive, since, in this case, the general solution includes an exponential term that grows with time. Notice that $\lambda_1$ and $\lambda_2$ always have a negative real part, due to the presence of the damping term $\mu_2 > 0$ of the oscillator 2. These two roots are independent of oscillator 1, and correspond to the case of oscillator 2 in linear forced oscillations. It is therefore natural to have conditions of stability for these two roots. However, if one calculates the product of the other two roots:

$$\lambda_3\lambda_4 = -\frac{\mu_2\beta_{12} a_2}{2\omega_1} \sin\gamma_2 - \frac{\beta_{12}^2 a_2^2}{8\omega_1^2} \sin^2\gamma_2, \tag{8.101}$$

and considering the first equation in (8.97) we see that some situations may occur where the product $\lambda_3\lambda_4$ is strictly less than 0, i.e., where at least one of these two (real) roots is positive. A detailed calculation shows that this instability condition is satisfied if:

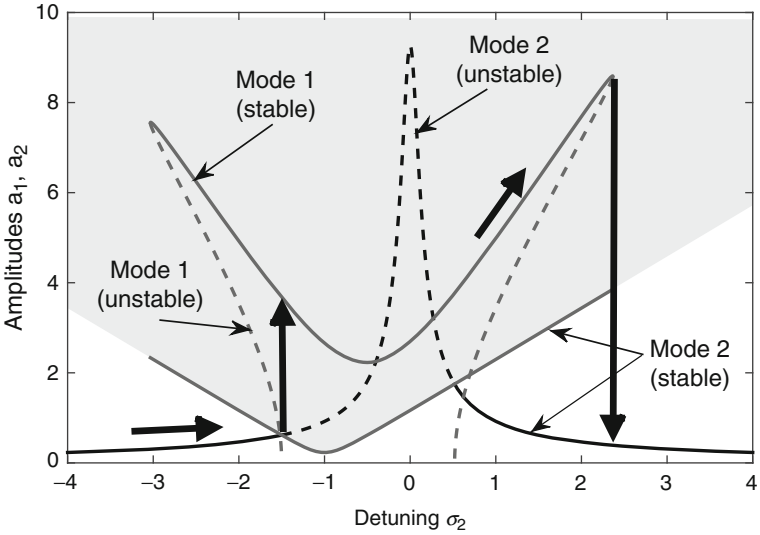


**Fig. 8.21** Amplitudes $a_1$ and $a_2$ of two nonlinearly coupled oscillators, as a function of the external detuning parameter $\sigma_2$. The *gray area* represents the instability domain. The *arrows* indicate the path of the running point when moving on the frequency axis ($\sigma_2$) from left to right. The *dashed lines* correspond to unstable parts of the resonance curves, and the *solid lines* to stable parts

$$a_2 > \frac{2\omega_1}{|\beta_{12}|}\sqrt{4\mu_1^2 + (\sigma_1 + \sigma_2)^2}. \tag{8.102}$$

The instability zone corresponding to (8.102) is shown in gray color in Fig. 8.21. Notice that the amplitude threshold increases with the damping of oscillator 1, and as the frequency moves away from $\omega_2$ ($\sigma_2 = 0$).

### Amplitudes and Phases of the Solution

After this analysis, we are now able to complete the study by calculating the amplitudes $a_1$ and $a_2$, and the phases $\theta_1$ and $\theta_2$. As a result, the zero-order solution is obtained, whose general form was specified in (8.92). Combining (8.92) with (8.94), and considering the definitions of $T_1$, $\sigma_1$, $\sigma_2$ $\gamma_1$ and $\gamma_2$, we get

$$\begin{cases} x_{10} = a_1 \cos(\omega_1 t + \theta_1) = a_1 \cos\left(\dfrac{\Omega}{2}t - \dfrac{\gamma_1 + \gamma_2}{2}\right), \\ x_{20} = a_2 \cos(\omega_2 t + \theta_2) = a_2 \cos\left(\Omega t - \gamma_1\right). \end{cases} \tag{8.103}$$

By solving the system (8.97) corresponding to stationary solutions, the amplitudes are finally obtained as a function of the input parameters:

$$\begin{cases} a_2 = \dfrac{2\omega_1}{|\beta_{12}|}\sqrt{(\sigma_1+\sigma_2)^2+4\mu_1^2}, \\ a_1 = 2\left[-\Gamma_1 \pm \sqrt{\dfrac{P^2}{4\beta_{21}^2}-\Gamma_2^2}\right]^{1/2}, \\ \text{with} \quad \Gamma_1 = \dfrac{2\omega_1\omega_2}{\beta_{12}\beta_{21}}\left[2\mu_1\mu_2-\sigma_2(\sigma_1+\sigma_2)\right], \\ \text{and} \quad \Gamma_2 = \dfrac{2\omega_1\omega_2}{\beta_{12}\beta_{21}}\left[2\mu_1\sigma_2-\mu_2(\sigma_1+\sigma_2)\right]. \end{cases} \tag{8.104}$$

The expressions (8.103) show an important result, as expected: for steady-state oscillations, the frequency of the oscillator 2 is equal to the excitation frequency $\Omega$, and the frequency of the oscillator 1 is exactly $\Omega/2$. This result is in accordance with the properties of internal resonance of the structure.

Figure 8.21 shows the curves of the amplitudes $a_1$ and $a_2$ of the coupled oscillators, as a function of the external detuning parameter $\sigma_2$, all other parameters being assumed to be constant. If the driving frequency increases (from left to right on the frequency axis), the following phenomena are observed:

1. First, the amplitude $a_2$ of oscillator 2 is examined. As long as the operating point is below the zone of instability, there is no subharmonic.
2. For the threshold value corresponding to the instability limit given by (8.102), the oscillator 1 suddenly appears. In the example shown, the amplitude $a_1$ is larger than $a_2$, and this remains true as long as the running point stays above the limiting instability curve.
3. As the maximum of the oscillator 1 curve is reached, the running point jumps back to the oscillator 2 curve, and the oscillation at $\Omega/2$ disappears.
4. If the frequency axis is described in the opposite direction by gradually reducing the excitation frequency, one observes qualitatively similar phenomena, but, in this case, the threshold values for which oscillator 1 appears are different. This is a characteristic *hysteresis* phenomenon.

## *8.5.5 Nonlinear Mechanical Model*

### 8.5.5.1 Introduction

The purpose of this section is to show that the fundamental properties of gongs and cymbals can be described by a set of nonlinearly coupled oscillators, similar to the above-presented example. To do this, the study starts by examining a nonlinear model of flexural vibrations for a spherical shallow shell. In fact, almost all gongs and cymbals show a rotational symmetry, and a more or less pronounced curvature. A spherical cap has similar properties and is a suitable approximation of real shapes

observed in gongs and cymbals. Compared to real instruments, some discrepancies will be observed on modal frequencies and shapes, but the general results will be preserved. In addition, the spherical shape has the advantage of providing an analytic reference model.

The case of thin spherical shallow shells is considered here in the context of large amplitude oscillations. The same notation as in Sect. 3.5.4 of Chap. 3 is used. These assumptions form the basis of the Von Kármán equations (also called, sometimes, equations of Marguerre or Koiter in the specialized literature) [1, 63]. Hamdouni and Millet, in particular, have shown that these equations can be obtained from an asymptotic method applied to the general equations of elasticity [33]. As in the linear case (see Sect. 3.5.4 in Chap. 3), the equations of motion are written in polar coordinates, where $(r, \theta)$ are the coordinates of one current point of the shell, after projection on the horizontal plane. These equations are written [63]:

$$\begin{cases} \nabla^4 w + \dfrac{\nabla^2 F}{R} + \rho h \ddot{w} = L(w, F) - \mu \dot{w} + p, \\ \nabla^4 F - \dfrac{Eh}{R} \nabla^2 w = -\dfrac{Eh}{2} L(w, w), \end{cases} \tag{8.105}$$

where $F$ is the Airy stress function, and $L$ a bilinear quadratic operator, written in polar coordinates:

$$L(w, F) = w_{rr} \left( \frac{F_r}{r} + \frac{F_{\theta\theta}}{r^2} \right) + F_{rr} \left( \frac{w_r}{r} + \frac{w_{\theta\theta}}{r^2} \right) - 2 \left( \frac{w_{r\theta}}{r} - \frac{w_\theta}{r^2} \right) \left( \frac{F_{r\theta}}{r} - \frac{F_\theta}{r^2} \right). \tag{8.106}$$

In Eq. (8.105), $F$ contains both linear and quadratic terms in $w$. As a consequence, $L(w, F)$ contains quadratic terms and cubic terms in $w$. Finally, the equation of flexural motion contains linear terms, quadratic terms and cubic terms in $w$. When $R \to \infty$, Eq. (8.105) represents the nonlinear flexural vibrations of a flat plate. In this case, the quadratic terms disappear, and only the cubic terms remain. To examine the relative significance of the different terms in these equations, it is necessary to write them in dimensionless form using the following variables [63]:

$$\begin{aligned} &r = a\bar{r}\,, \quad t = a^2 \sqrt{\rho h / D}\,\bar{t}\,, \quad w = h^3 / a^2 \overline{w}\,, \quad F = Eh^7 / a^4 \overline{F}\,, \\ &\mu = [2Eh^4 / Ra^2] \sqrt{\rho h / D}\,\overline{\mu}\,, \quad p = Eh^7 / Ra^6 \overline{p}. \end{aligned} \tag{8.107}$$

Thus Eq. (8.105 ) becomes[14]

[14]For the sake of clarity, the overlinings are now removed from the equations.

$$\begin{cases} \nabla^4 w + \varepsilon_q \nabla^2 F + \ddot{w} = \varepsilon_c L(w, F) + \varepsilon_q \left[ -\mu \dot{w} + p \right], \\ \nabla^4 F - \dfrac{a^4}{Rh^3} \nabla^2 w = -\dfrac{1}{2} L(w, w). \end{cases} \tag{8.108}$$

Equations (8.108) contain a quadratic perturbation coefficient $\varepsilon_q = 12(1-\nu^2)h/R$ and a cubic perturbation coefficient $\varepsilon_c = 12(1-\nu^2)h^4/a^4$. Within the framework of "thin shell" approximations, i.e., $h \ll a$ and $hR \ll a^2$, one can see that the cubic terms are significantly smaller than the quadratic terms. In practice, this means that even a very small curvature of the structure allows the quadratic nonlinearities to dominate. This may explain why it is extremely difficult, or even impossible, to experimentally exhibit the phenomena of cubic nonlinearity on a plate: even the slightest flatness defect has such effect that the cubic nonlinear term is masked by the quadratic one.

The nonlinear solution is now expanded onto the basis of the eigenmodes, taking advantage of their orthogonality properties[15]:

$$w(r, \theta, t) = \sum_n \Phi_n(r, \theta) q_n(t). \tag{8.109}$$

As a consequence, all nonlinear terms will appear in the time functions (generalized displacements). These functions form a system of coupled differential equations:

$$\ddot{q}_n + \omega_n^2 q_n = \varepsilon_q \left[ -\sum_p \sum_q \alpha_{npq} q_p q_q - \mu \dot{q} + p_n \right] + \varepsilon_c \sum_p \sum_q \sum_r \beta_{npqr} q_p q_q q_r, \tag{8.110}$$

which highlights the simultaneous existence of cubic and quadratic coupling terms. For a plate, the coefficients $\alpha_{npq}$ are all equal to zero. For a shell, we note a formal analogy between these results and those obtained for the pendulum (see Sect. 8.1). The quadratic nonlinearity here results from the asymmetry due to the curvature.

The expansion of the shell motion in terms of eigenmodes is only one possible way of representing the solution, and this does not imply any linearity of the problem. In contrast to the linear case, it is not possible to decouple the differential equations that govern the time functions $q_n(t)$. In addition, this representation does not imply at all that the deflection shape of the shell for $\omega = \omega_n$ is the (linear) mode shape $\Phi_n(r, \theta)$. This can be seen, for example, by rewriting Eq. (8.110) under forced oscillations at this frequency. In general, the vibratory motion of the shell for a given frequency depends on the amplitude. Because of intermodal couplings (see Sect. 8.5.4), the deflection shape of the shell, for given loading frequency and amplitude, is a complex combination of several mode shapes (see Fig. 8.24 in the next section).

[15] Details on numerical methods for solving the von Kármán plate equations can be found in [8].

#### 8.5.5.2 Truncation

If the nonlinearities are weak, and if the forcing frequency is close to one particular eigenfrequency, it is legitimate to truncate the system (8.110) by keeping only the equations that govern the main excited modes, and those associated with them through internal resonances. Let us illustrate this by the example of a thin spherical shell shown in Fig. 8.22. This example shows a situation where the structure is excited at its center with frequency $f \simeq f_3 = 224\,\text{Hz}$, corresponding to the

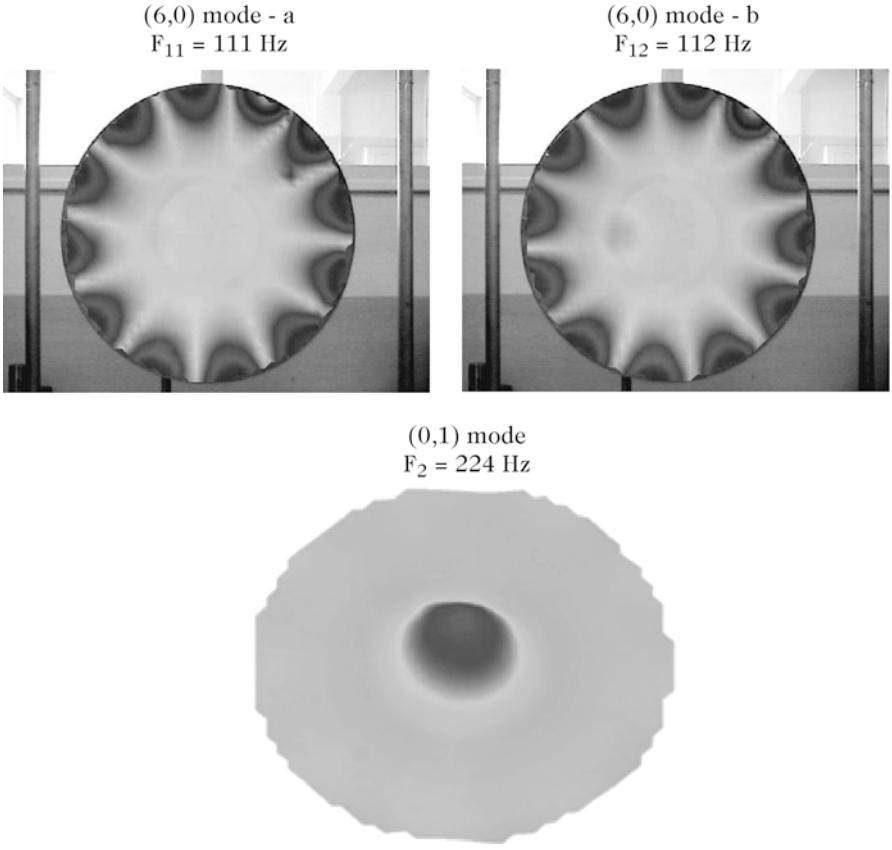


**Fig. 8.22** Examples of some particular modes of a spherical shell subjected to internal resonance (see also [64])

symmetric mode (0,1).[16] For this particular shell, it turns out that the frequency of the mode (0,1) corresponds to twice the asymmetric modal frequencies (6,0), approximatively: $f_1 = 111\,\text{Hz}$ and $f_2 = 112\,\text{Hz}$.

In order to observe the phenomena caused by a forcing in the vicinity of $f_{01}$, then it can be assumed that the displacement is written in the approximated form:

$$w(r,\theta,t) \simeq \Phi_{60}(r)\left[q_1(t)\cos 6\theta + q_2(t)\sin 6\theta\right] + \Phi_{01}(r)q_3(t). \tag{8.111}$$

where $q_1$ and $q_2$ are the generalized displacements corresponding to the two configurations in quadrature for the asymmetric modes (6,0), and where $q_3$ governs the temporal evolution of the axisymmetric mode (0,1). As a consequence of the modal truncation, the system (8.110) is written in reduced form as follows:

$$\begin{cases} \ddot{q}_1 + \omega_1^2 q_1 = \varepsilon_q\left[-\beta_{13}q_1q_3 - 2\mu_1\dot{q}_1\right], \\ \ddot{q}_2 + \omega_2^2 q_2 = \varepsilon_q\left[-\beta_{23}q_2q_3 - 2\mu_2\dot{q}_2\right], \\ \ddot{q}_3 + \omega_3^2 q_3 = \varepsilon_q\left[-\beta_{11}q_1^2 - \beta_{22}q_2^2 - 2\mu_3\dot{q}_3 + P_3(t)\right]. \end{cases} \tag{8.112}$$

where $P_3(t)$ represents the forcing term, and where terms of modal damping of the form $-2\mu_i\dot{q}_i$ are added. The cubic terms are ignored because of the "thin shell" assumptions, as discussed previously. The intermodal coupling coefficients $\beta_{ij}$ depend on both the geometrical and material properties of the shell. These parameters can be calculated explicitly [63]. The resolution of the nonlinear system (8.112) can be made using the method of multiple scales presented in Sect. 8.5.4.

Figure 8.23 shows the stability curve obtained for the truncated system (8.112). The theoretical results are represented by solid lines (where the states are stable) or dotted lines (when unstable). The experimental points are represented by triangles and circles. One sees at the center of the figure the classical resonance curve of a forced isolated oscillator close to its eigenfrequency. This is the curve that would have been obtained for an isolated oscillator (0,1), with no internal resonances related to other modes. By changing the driving frequency, one obtains different coupling situations of this mode with one configuration of the two asymmetric modes (6,0). Figure 8.24 illustrates these nonlinear couplings for a spherical shell excited at its center: in each case, one can see the simultaneous contributions of the axisymmetric mode and an asymmetric mode.

[16] As shown in Chap. 3 for the circular membrane (see Fig. 3.32), a mode $(n, m)$ of a structure with a circular geometry is characterized by $n$ nodal diameters and $m$ nodal circles. However, in contrast to the case of stretched membranes described in Chap. 3, the outer edge of the spherical shells considered here are free, so that the lowest number of nodal circles is zero.

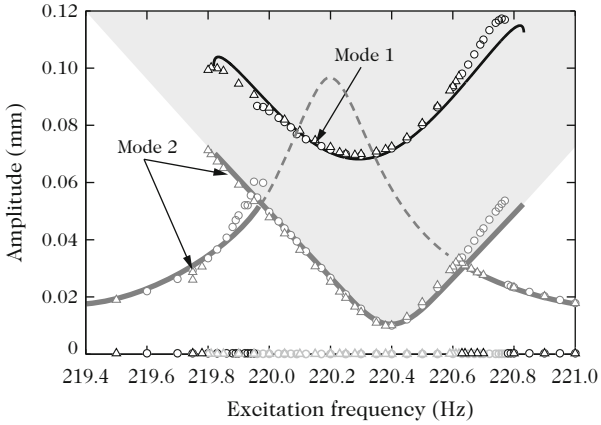


**Fig. 8.23** Stability curve for a thin spherical shell excited close to the frequency of mode (0,1). *Black*: response of mode (0,1). *Gray*: responses of both configurations for the mode (6,0). *Solid lines and dotted lines*: theoretical model (8.112). *Triangles and circles*: experimental points. After [64]

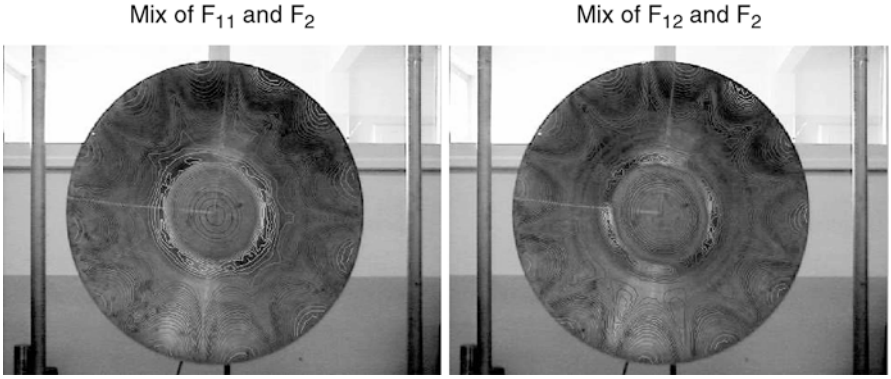


**Fig. 8.24** Examples of large amplitude deflection shapes of a spherical shell driven at its center. This figure shows two situations of coupling between the axisymmetric mode (0,1) and one configuration of the asymmetric modes (6,0) shown in Fig. 8.22. See also [64]

#### 8.5.5.3 Generalization and Musical Interest

The previous section allows us to understand a key aspect of sound generation in gongs and cymbals where the spectrum shows new components above a given threshold of amplitude, as a consequence of geometric nonlinearity. At the end of the Sect. 8.5.5 the presentation was deliberately focused on the interaction between a small number of modes. However, these results can be quantitatively generalized to a non-sinusoidal periodic forcing, which is coherent with the reality as one observes in practice the distortion of the response even for low excitations (see Sect. 8.5.1).

In this case, the enrichment of the spectrum is due to combinations of modes around each harmonic of the driving signal. Sound synthesis of gongs and cymbals based on these methods were made by Ducceschi and Touzé [23].

As said earlier, the normal excitation of a cymbal or a gong is a force impulse, communicated to the structure by the impact of a mallet (or a stick). The spectrum of the impact force is analogous to that of a low pass filter, whose bandwidth increases with the hardness of the mallet's head. For a pulse excitation, the system (8.112) can only be solved numerically, since the nonlinearities do not obey the principle of superposition. At this stage, one can imagine that each component of the excitation spectrum gives rise to a local spectral broadening and that, in total, there is an energy transfer to the high frequencies, beyond the initial spectrum. That is what is audibly observed, and confirmed by experiments.

## 8.6 Chaotic Regime

Let us now return to the fundamental experience described in Fig. 8.17. In the previous sections, the phenomena observed between the two bifurcations were studied. Beyond the second bifurcation, the observed acceleration of the gong (or of the cymbal) shows a broadband spectrum where it is no longer possible to discriminate between the discrete frequency peaks. The Fourier transform is not the right tool to describe the dynamics of the system properly, and other methods of analysis must be considered. Details of the transition to chaos in thin structures can be found in [69].

Among the possible strategies, observing the signal in the phase space is an effective and recognized method for analyzing the dynamics of nonlinear systems [27, 48]. Starting from a given time series $s(t)$, the phase space trajectory is obtained by representing the set of points with coordinates $[x_1 = s(t), x_2 = s(t+T)]$ where $T$ is a time delay whose value obeys selection criteria that are beyond the scope of the present book. One can remember that a widely used method consists of choosing $T$ as equal to the first zero of the autocorrelation function of the signal. Another possibility is to select the first minimum of the mutual information function. The reader interested in these questions can see for instance [40].

Figure 8.25 shows a comparison between a standard spectral representation and a phase space representation, for a cymbal vibration signal, where the instrument is excited by a sinusoidal force, for three different forcing amplitude, successively. As long as the amplitude remains weak, the spectrum is harmonic, and the trajectory takes the form of a closed curve. When the forcing amplitude increases, one can see an inharmonic spectrum due to the multiple combinations of resonances whose origin has been described earlier in this chapter. Here, the phase space trajectory shows typical foldings, which are known to indicate a possible route to chaos. Finally, after a second bifurcation, the spectrum is almost continuous, and the phase space representation takes the form of a blurring structure, which is difficult to analyze visually. We will see below how to draw valuable information from this signal.

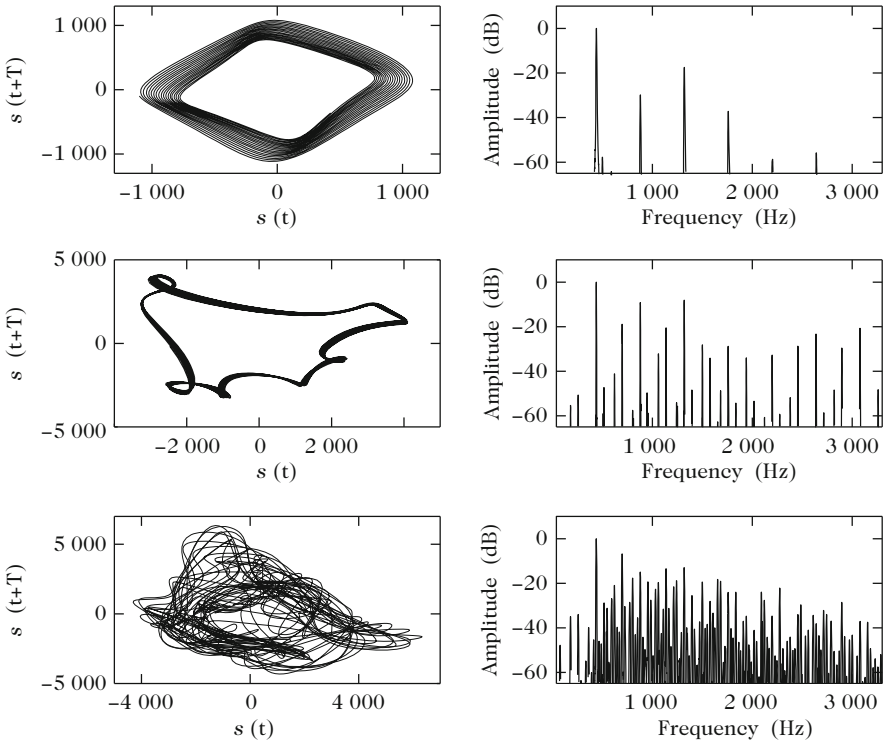


**Fig. 8.25** Phase space and spectrum of a sound for a cymbal under sinusoidal forcing excitation at 440 Hz. *Top line*: quasi-linear oscillations. *Medium line*: weakly nonlinear oscillations. *Bottom line*: chaotic regime

### *8.6.1 Degrees of Freedom*

The erratic structure of the cymbal vibrations at the bottom of Fig. 8.25 looks like a random signal. However, random signals are characterized by a lack of correlation between successive time windows of the signal. Therefore, it is of interest to check whether or not such a correlation exists here. For this purpose, the signal $s(t)$ is sampled at regular intervals $t_n = nT_e$ (where $n$ is a positive integer), and the obtained time series is denoted $s(n)$. $N$ indicates the length of $s(n)$. Then, a set of vectors $y(n)$ is built, defined by:

$$\begin{aligned} &y(n) = [s(n), s(n + n_T), s(n + 2n_T), \ldots, s(n + (d-1)n_T)] \\ &\text{with } n = 1, \ldots, N - (d-1)n_T, \end{aligned} \tag{8.113}$$

where the parameter $d$ is called the *embedding dimension* of the vectors $y(n)$, and where the index $n_T$ corresponds to the time delay $T$ used for representing the signal

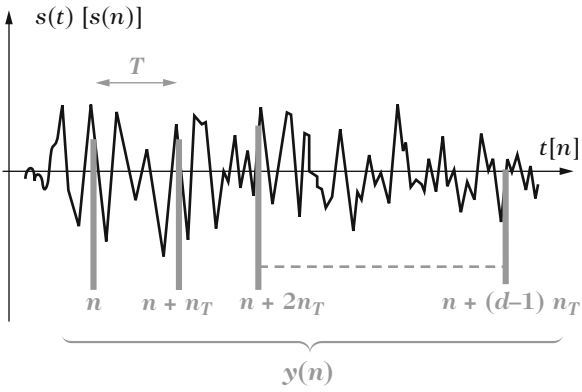


**Fig. 8.26** Creation of a multivariate set from a time series

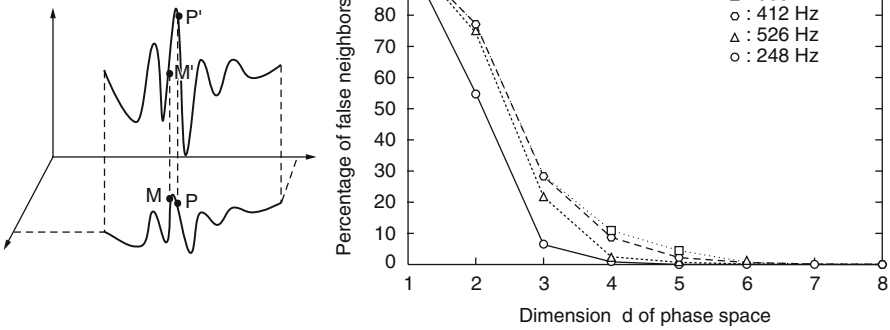


**Fig. 8.27** (*Left*) Principle of signal "unrolling" in phase spaces of increasing sizes: the points $M$ and $P$ are neighbors in dimension 2, but are no longer neighbors in dimension 3. (*Right*) Percentage of false neighbors as a function of the dimension $d$ of the space for cymbal vibrations, at different excitation frequencies

in phase space. In total, the length of $s(n)$ required for the construction of each vector $y$ is equal to $dn_T$. If we want to explore $s(n)$ entirely, it is necessary to make $n$ varying within the interval 1 to $N-(d-1)n_T$. Figure 8.26 illustrates the partition of the initial series $s(n)$.

This partition might seem arbitrary at first sight. In practice, it will be used to check whether $s(n)$ is random or deterministic. We will also derive a first estimate of the number of degrees of freedom of the underlying mechanical system from this analysis.

A first method is presented, called *method of false nearest neighbors*. To illustrate it, let us examine the case $d = 2$. This corresponds to the case of the phase space shown in Fig. 8.25, where the components of vector $y(n)$ are $s(n)$ and $s(n + n_T)$. These components are the coordinates of a point $M$ on the trajectory (see Fig. 8.27). Let us consider this point and another *neighbor* point $P$ on the same trajectory.

Imagine now that we examine the case $d = 3$: for that purpose, the cymbal motion is now represented in a three-dimensional space, where the vector $y(n)$ has three components $s(n)$, $s(n+n_T)$, and $s(n+2n_T)$. One can see this procedure as unrolling a 2-D "ball of wool" into 3D! The central question is to know if, during this operation, M and P will remain close neighbors or not. In the case of a random signals, it can be shown that close neighbors in dimension $d$ never stay close in dimension $d + 1$. This is a property of *false nearest neighbors*. With a deterministic signal, similar to those we are interested in here, the number of false neighbors regularly decreases as $d$ increases (see Fig. 8.27).

Figure 8.27 shows that the percentage of false neighbors is practically zero beyond a certain value of $d$ ($d = 8$ here). This means that, for this dimension, the trajectory is completely unrolled, and that the projection into a space of higher dimension does not provide any additional information: for $d > 8$, all neighbors are "true neighbors" which stay close if $d$ increases. This is also the case for a mechanical system of finite dimension $m$: if one attempts to use $m + 1$ variables to describe this system, it necessarily leads to a set of equations where one variable is expressed as a function of the $m$ others, and we have only $m$ independent equations. To sum up, the method of false nearest neighbors described here gives an upper boundary for the dimension of the system from which the time series $s(n)$ was extracted. According to this estimation, we would derived here $m \leq 8$ for the cymbal dynamics.

An estimation of the lower boundary of $m$ can be obtained by calculating the *correlation dimension*. This is obtained by determining the number of pairs of points whose mutual distance is smaller than a certain quantity $\varepsilon$. For a series of points $N$, the discrete formulation of the *correlation integral* is written:

$$C(\varepsilon) = \frac{1}{N(N-1)} \sum_{i \neq j} H\left(\varepsilon - \|y(i) - y(j)\|\right), \tag{8.114}$$

where the vectors $y$ of dimension $d$ are calculated like as the method of false neighbors described above. $H$ is the Heaviside function.

Figure 8.28b represents, in logarithmic coordinates, the correlation integral $C(\varepsilon)$ depending on $\varepsilon$ for increasing values of the dimension $d$, in the case of cymbal vibrations. It can be seen that the slope of this curve increases, and tends to a limiting value from a given value of $d$ (around $d = 6$ in this figure). This is a general result, which is also valid for other dynamical systems [31]. This property means that, beyond this limiting value, the number of pairs of points increases exponentially with a constant exponent $d_c$ ($C(\varepsilon) \sim \varepsilon^{d_c}$), regardless of the value of $d$. This also means that the relative increase $\mathrm{d}dC/C$ is proportional to the relative increase of the "radius" $\mathrm{d}d\varepsilon/\varepsilon$. The asymptotic value $d_c$ of the slope is the *correlation dimension of the system*.

This behavior characterizes a deterministic dynamical system with a finite number of degrees of freedom. In the case of a random signal, a white noise, for

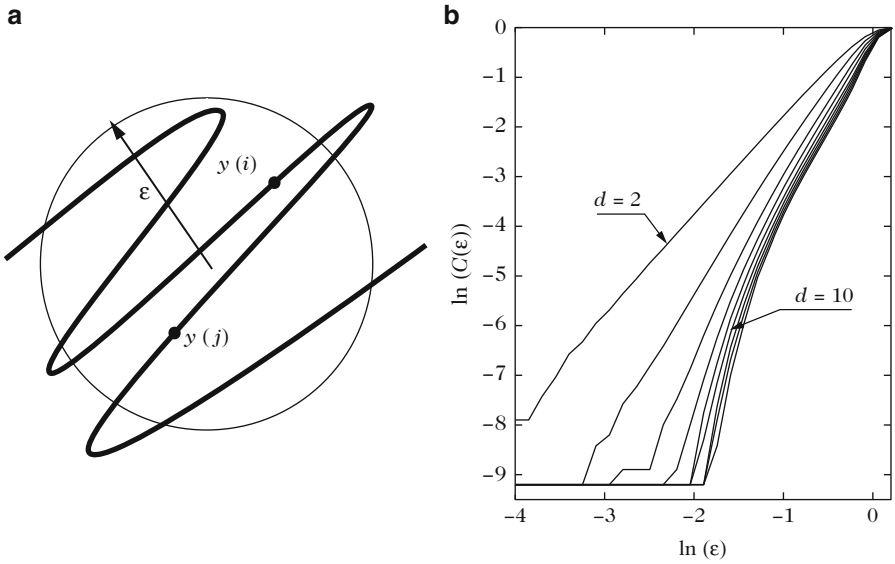


**Fig. 8.28** Correlation integral. (**a**) Principle of the calculation: for a given dimension $d$, the number of pairs of points is evaluated whose distance is less than a given quantity $\varepsilon$. (**b**) Correlation integral $C(\varepsilon)$ of cymbal vibrations, for $d$ varying between 2 and 10

example, we would observe that the slope of $\ln[C(\varepsilon)]$ continues to increase with increasing values of $d$. This would mean, in practice, that the relative increase in the number of pairs of neighboring points within a hypersphere of radius $\varepsilon$ continues to grow faster than the relative increase of the radius when the signal is observed in spaces of increasing dimensions.

Figure 8.29 shows a range of estimates of $d_c$ obtained from multiple vibration recordings of the same cymbal, for various forcing frequencies and excitation positions. We note that the correlation dimension converges for all signals, which is a clear indication of a deterministic process governed by a small number of degrees of freedom (DOF). However, we note that $d_c$ is not identical in all cases, suggesting that the number of DOF depends on both the driving frequency and excitation position. This result is in accordance with the mechanical analysis of the problem made earlier in this chapter.

In conclusion, is has been shown in this section that some analysis tools exist for extracting information from signals governed by highly nonlinear process, for which conventional spectral analysis is no more applicable. From a practical point of view, the quality of the estimates can be rapidly affected if the signal is corrupted by noise. In addition, it is often necessary to analyze signals of long duration ($N$ large) in order to obtain results with a sufficient accuracy. In any case, the estimation of the dimensions should be connected to a physical analysis of the phenomena, in order to avoid hazardous interpretations.

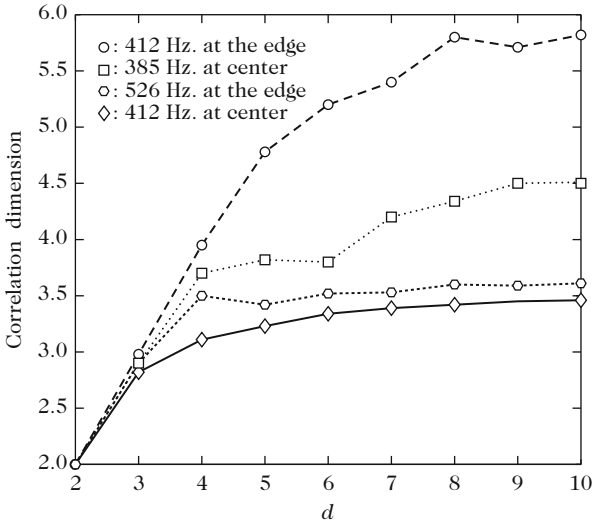


**Fig. 8.29** Correlation dimension of some cymbal vibration signals as a function of the dimension $d$, for various driving frequencies and observation positions. Notice that the correlation dimensions $d_c$ of all signals converge to an asymptotic value

## *8.6.2 Characterization of Chaos: Lyapunov Exponents*

In the previous sections, the term "chaotic" was used to characterize the vibratory oscillations of cymbals and gongs subjected to strong nonlinear oscillations. This concept will be now made clearer and a method will be presented for quantifying the chaos.

A chaotic system is mainly characterized by its sensitivity with regard to the initial conditions. For a deterministic system, one can exactly reproduce the temporal variations of a variable, provided that the same initial conditions are given. With a chaotic system, even a small perturbation of these conditions is sufficient for the system to operate on a completely different trajectory in the phase space. The *Lyapunov exponents*, which are calculated from measured samples of a time series $s(n)$ (see the next section), are quantities that measure the divergence rate of small perturbations around a given trajectory in phase space accurately, and are recognized as pertinent to quantify the chaos. Only one positive exponent is sufficient for the trajectory to diverge, which proves the sensitivity of the system to initial conditions.

### 8.6.2.1 Calculation of the Lyapunov Exponents

The presentation below is inspired by Manneville [43]. As for the estimation of dimensions discussed above, we start from a time series $s(n)$ (with $n = 1, \ldots, N$) from which a set of vectors $y(n)$ is constructed, using the procedure described

in (8.113). At a future time $T_F = n_F T_e$, which is assumed to be small, the vectors $y(n)$ are transformed into another set $y(n + n_F)$. The calculation of the Lyapunov exponents is then made on the function $\mathbf{F}$ which characterizes the evolution of $y(n)$ to $y(n + n_F)$, which can be written symbolically[17]:

$$y(n + n_F) = \mathbf{F}\{y(n)\}. \tag{8.115}$$

As an illustration, let us consider the simple case of a single variable with initial condition $y_0$. First, we choose $n_F = 1$. Introducing a small initial perturbation, we obtain the adjacent trajectory $\tilde{y}_0 = y_0 + \delta y_0$. From (8.115) it gives

$$\begin{aligned} \tilde{y}_1 = y_1 + \delta y_1 &= \mathbf{F}(\tilde{y}_0 = y_0 + \delta y_0) \\ &= \mathbf{F}(y_0) + \mathbf{F}'(y_0)\delta y_0. \end{aligned} \tag{8.116}$$

Thus, the distance $|\delta y_1|$ between two trajectories is given by $|\delta y_1| = |\mathbf{F}'(y_0)||\delta y_0|$. Pursuing the same calculation to the next iteration gives

$$|\delta y_2| = |\mathbf{F}'(y_1)||\mathbf{F}'(y_0)||\delta y_0|. \tag{8.117}$$

Finally, after $n_F$ iterations, we get

$$|\delta y_{n_F}| = \left( \prod_{k=0}^{k=n_F-1} |\mathbf{F}'(y_k)| \right) |\delta y_0|. \tag{8.118}$$

It can be seen in (8.118) that the required quantity is obtained, namely a measure of the evolution of the perturbation. This evolution can be quantified by a global coefficient $\gamma$ defined as follows:

$$\gamma^{n_F} = \frac{|\delta y_{n_F}|}{|\delta y_0|}. \tag{8.119}$$

Finally, the Lyapunov exponent $\lambda$ is defined as the logarithm of $\gamma$, which yields

$$\lambda = \ln(\gamma) = \frac{1}{n_F} \sum_{k=0}^{n_F-1} \ln |\mathbf{F}'(y_k)| \tag{8.120}$$

for an estimation on $n_F$ iterations. If the exponent $\lambda$ defined in (8.120) is positive, this means that, for different initial conditions, the trajectories diverge as $e^{\lambda n}$, or, equivalently, as $e^{\lambda t}$ using the dimensional quantities.

[17] The choice of $T_F$ determines the accuracy of the estimated Lyapunov exponents. These very technical considerations will not be detailed here, and we invite the interested reader to refer to the specialized literature [40, 43]. We simply recommend to choose $T/2 \leq T_F < T$, where $T$ is the time interval chosen for the construction of the vectors $y$ [see Eq. (8.113)].

The previous calculus can be generalized to higher values of the dimension $d$ (dimension of vectors $y$) without any difficulties. In this case, several Lyapunov exponents are obtained. This is known as the *Lyapunov spectrum*. These exponents are calculated from the Jacobian of the transformation $\mathbf{F}$ [43, 67]. Only one Lyapunov exponent needs to be positive for the trajectories to diverge, and one can then conclude that the system is chaotic. Such properties are observed in the case of cymbals and gongs, and this result comes in addition to other analysis methods (mechanical model, phase space, bifurcations,...) to explain the scenario of routes to chaos for these instruments, subjected to large amplitude oscillations [14].

Finally, since the transformation for vibrations to acoustic waves is linear for percussion instruments, all nonlinearities are contained in the vibrations. In other words, the considerations presented in this chapter remain valid to explain the observations made on the sounds of cymbals and gongs. On the experimental point of view, it is preferable to perform the analysis on the vibration of one particular point of the structure rather than on the radiated sound. In fact, the combinations of modes and the number of degrees of freedom vary from one point to another of the structure. As the sound pressure results from an integration over the whole geometry, it is understandable that the corresponding signals are therefore more difficult to analyze.

## 8.7 Nonlinear Normal Modes

### *8.7.1 Introduction*

As soon as the nonlinearities are considered in a physical problem, then the evolution equations of the variables are coupled together. This has been seen on several occasions in this chapter, as, for example, in Eq. (8.110) for gongs and cymbals. The superposition theorem, which enables us to solve several simple problems independently, and then to reconstruct the overall response by summing individual responses, is no longer valid. As a consequence, it becomes also difficult, or even impossible, to make truncations in the system. Terms that would be otherwise neglected could be responsible for major changes in the evolution of the system, whereas such simplifications are perfectly justified in the linear case. Direct solving of nonlinear problems is often impossible analytically. It thus implies long and heavy numerical calculations, which are very demanding in terms of computational resources. However, in many situations, the dynamics observed in real cases seem to be relatively simple. This is, for example, the case for a structure forced near its resonance frequency, at moderate amplitudes. Even if nonlinearity is present, yielding higher harmonics and bending of resonance curves like those shown in Sect. 8.2, the dynamic behavior remains rather simple to describe.

In order to propose effective methods to reduce the nonlinear dynamics in specific cases, the concept of *nonlinear normal mode*, or NNM, was introduced.

This concept is briefly presented below, for the particular case of a vibrating structure under large amplitude, i.e., for geometric nonlinearities. It is assumed that the modes of the system were calculated in a previous step, and that the equation of motion was projected onto these modes, so that the starting point of this presentation is a dynamical system of the form shown in (8.110), i.e., an infinite number of nonlinearly coupled oscillators. Damping and forcing terms are left aside in this presentation.

### 8.7.2 First Approach of Nonlinear Normal Modes

To make the reader understand the interest of NNMs, we will present this concept on a simple case. The selected example is the dynamics of a mass subjected to elastic restoring forces by two springs whose extensions are not considered as small, so that linear approximations are not justified here (Fig. 8.30).

$l_0$ is the length of the springs at rest. The coordinates of the point mass $m$ at time $t$ are $l_0 + x_1$ and $l_0 + x_2$, respectively. The problem is expressed in terms of the dimensionless variables $X_1 = x_1/l_0$ and $X_2 = x_2/l_0$. We denote $\omega_1^2 = k_1/m$ and $\omega_2^2 = k_2/m$ the square of the natural angular frequencies of the system, corresponding to purely horizontal and vertical motions in the physical space $(X_1, X_2)$, respectively. The elastic potential energy $W$ of the system is given by:

$$W = m\left\{\frac{1}{2}\omega_1^2\left[X_1 + \frac{1}{2}\left(X_1^2 + X_2^2\right)\right] + \frac{1}{2}\omega_2^2\left[X_2 + \frac{1}{2}\left(X_1^2 + X_2^2\right)\right]\right\}. \tag{8.121}$$

The equations of motion are then obtained by:

$$m\ddot{X}_i + \frac{\partial W}{\partial X_i} = 0, \qquad \text{for} \quad i = 1, 2. \tag{8.122}$$

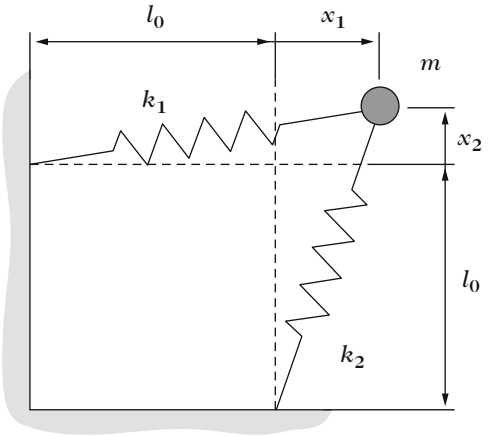


**Fig. 8.30** A point mass $m$ is fixed at two springs of stiffness $k_1$ and $k_2$, respectively. Each spring is rigidly fixed to the other end of the walls, which are perpendicular to each other

Finally, the equations governing the dynamics of the system are written:

$$\begin{aligned}
&\ddot{X}_1 + \omega_1^2 X_1 + \frac{\omega_1^2}{2}(3X_1^2 + X_2^2) + \omega_2^2 X_1 X_2 + \frac{\omega_1^2 + \omega_2^2}{2} X_1 (X_1^2 + X_2^2) = 0, \\
&\ddot{X}_2 + \omega_2^2 X_2 + \frac{\omega_2^2}{2}(3X_2^2 + X_1^2) + \omega_1^2 X_1 X_2 + \frac{\omega_1^2 + \omega_2^2}{2} X_2 (X_1^2 + X_2^2) = 0.
\end{aligned} \tag{8.123}$$

Notice that both equations are decoupled in the linear regime, which is due to the fact that the modal variables, $X_1$ and $X_2$ were chosen to describe the system.

Truncation problems mentioned in the previous section can be easily illustrated with these equations. Suppose that we want to study the motion of the first mode, simplifying the system (8.123) by writing $X_2 = 0$. The dynamical problem that governs $X_1$ then yields an inconsistent result. In fact, if $X_1 \neq 0$, the term in $X_1^2$ of the second equation of (8.123) yields energy to the second oscillator, so that we no longer have $X_2 = 0$ !

However, if the system is linear, a motion initiated with the first eigenmode, taking as initial conditions $X_1 \neq 0$ and $X_2 = 0$, is such that $X_2$ remains equal to zero. This is the property of *invariance* of eigenmodes for a linear system. This is no longer true for nonlinear systems, because of the presence of terms such as $X_1^2$ in the second equation of (8.123). We are now able to define NNMs more accurately, but before that we need to specify the general framework.

### 8.7.3 Invariant Manifolds

Consider the dynamics of the system in phase space. For that purpose, the system (8.123) is written in first order, by using the velocities $Y_1 = \dot{X}_1$ and $Y_2 = \dot{X}_2$ as additional independent variables. The phase space thus is four-dimensional, and the dynamics can be rewritten as:

$$\begin{cases}
\dot{X}_1 = Y_1, \\
\dot{Y}_1 = f_1(X_1, Y_1, X_2, Y_2), \\
\dot{X}_2 = Y_2, \\
\dot{Y}_2 = f_2(X_1, Y_1, X_2, Y_2).
\end{cases} \tag{8.124}$$

The eigenmodes correspond to two hyperplanes defined by: $X_2 = Y_2 = 0$ for the first mode, $X_1 = Y_1 = 0$ for the second mode. These are two-dimensional subspaces of the phase space. These subspaces are not *invariant* (see the end of the previous section), this property being true if the dynamics is linear, only. This is illustrated in Fig. 8.31, where the system (8.123) is solved numerically for three different initial conditions on the first eigenmode, respectively: $X_1 = 0.01$, $X_1 = 0.025$,

and $X_1 = 0.05$, respectively (all other coordinates being equal to zero), and for an integration time $T$ corresponding to 12 times the period $T_1 = 2\pi/\omega_1$ of the first oscillator.

It is found that the first orbit (or periodic solution) is almost included in the plane defined by the first eigenmode. This trajectory was calculated for a small amplitude, $X_1 = 0.01$, the nonlinearities do not appear and the loss of invariance is almost not visible. This is not the case for the other two orbits, which are no longer included in the plane. The significant contribution that can be observed on the coordinate $X_2$ is entirely due to the coupling term in $X_1^2$ on the second equation that induces an energy transfer from the first to the second mode.

Let us now observe the computed trajectories for other initial conditions, selected at well-chosen locations in phase space. Figure 8.32 shows three trajectories, computed for the same observation time $T$, and which initial conditions are: $(X_1, X_2)$=(0.01,0) ; (0.025, $2.3 \times 10^{-5}$) and (0.05, $1.8 \times 10^{-4}$), respectively. Selected values of $X_2$ are small compared to those of $X_1$, and appear as small corrections brought for recovering out closed periodic orbits. These initial conditions have been selected onto the first NNM, and this allows us to define the NNM by two equivalent formulations. First, they can be defined as the family of periodic orbits existing in the vicinity of the origin. Existence of these periodic orbits are guaranteed by a theorem due to Lyapunov [42], and one can see in Figs. 8.31 and 8.32 that they are not confined into the linear eigenspaces but are slightly aside. This definition is however limited to the conservative case, as periodic orbits are no longer solutions of the dynamical system as soon as dissipation comes into play. To overcome

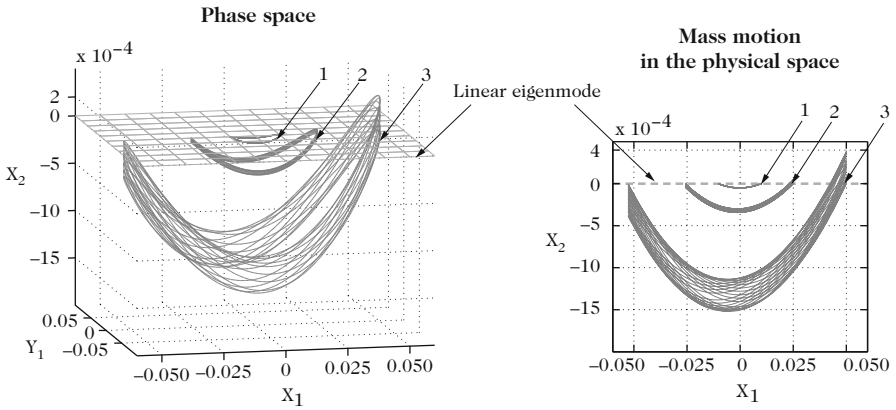


**Fig. 8.31** Non-invariance of the first eigenmode. The figure on the *left* shows the trajectories of the system in phase space $(X_1, Y_1, X_2)$. The plane $X_2 = 0$ corresponds to the first eigenmode. Three initial conditions were taken (numbered 1, 2, and 3), for $X_1 = 0.01$, $X_1 = 0.025$, and $X_1 = 0.05$. We see that the corresponding trajectories are located out of the plane defining the first eigenmode. The figure on the *right* shows the motion of the mass in the physical space $(X_1, X_2)$. Here, we have: $\omega_1 = 1$, $\omega_2 = \sqrt{2}$

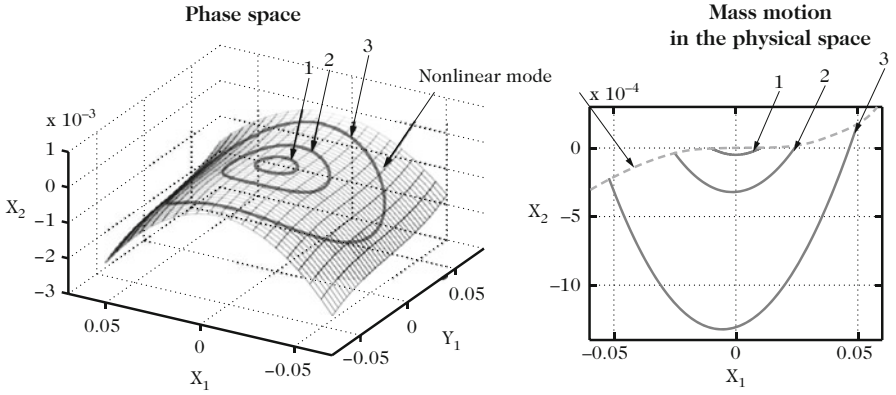


**Fig. 8.32** First nonlinear normal mode. On the *left*: representation in phase space, showing the invariance property of the nonlinear normal mode. For three different initial conditions (numbered 1, 2, and 3) taken on the manifold, the periodic orbits are entirely contained within the nonlinear normal mode. On the *right*: representation of the mass motion in the physical space $(X_1, X_2)$. The consequence of the invariance is that the motion of the mass occurs along a line and not on a blurred trajectory

this limitation, an NNM can be defined as the set of initial conditions giving rise to trajectories that are contained in a two-dimensional surface, or manifold in mathematical terms. By doing so, one introduces the fundamental notion of invariance. For a conservative system, the NNM can be viewed as the manifold generated by all the periodic orbits. This manifold is invariant because any initial condition taken on it will give rise to a trajectory that will stay on the manifold, for any time. This definition in terms of invariant manifold is more general and will be retained in the following.

We are now able to define an NNM:

**Definition.** An NNM is an invariant manifold (a surface) in the phase space, which is tangent to the corresponding eigenspace at the origin (corresponding to the position at rest). This definition ensures the following properties:

- Imposing that the manifolds be tangent at the origin to the eigenmode can help in recovering the linear results. The nonlinear modes are thus defined as an extension of the eigenmodes, where the invariance property is retained.
- The invariant manifolds are in fact minimal surfaces that allow us to capture existing trajectories of the phase space: making projections on these surfaces is therefore a priori the best possible reduction, which is their fundamental interest.
- With this notion, we are able to compute reduced-order models that retain the essential properties of the observed dynamics. We thus find the issue raised in the introduction: the apparent complexity of the equations, which needs to retain a large number of oscillators, is included in the curved geometry of the manifold. Now, the dynamics of that manifold is relatively simple, since it is governed by a single oscillator, that we will specify in the next section.

### 8.7.4 Calculation of Nonlinear Normal Modes

Several methods exist to calculate the NNMs. In this presentation, two of them are selected, that use powerful mathematical tools (encountered elsewhere in many other areas of physics) and that fully exploit the notions of invariance. The first work introducing the concept of NNM is due to Rosenberg [56], although without the more general interpretation in terms of invariant manifolds that was introduced here.

One first approach consists in calculating the geometry of the invariant manifold in the phase space, and then to project the equations of motion onto the manifold. To do this, a very general theorem of dynamical systems is used: the *center manifold* theorem. The results given by this theorem are of great significance, since it provides the best means of reducing nonlinear dynamics. The basic idea is to separate the very damped modes, which have a very short lifetime and have therefore little influence on long-term dynamics, from the lightly damped modes, which are primarily responsible for the dynamics over long duration. Once these two families are separated, it is shown that the center manifold of the phase space, which contains the amplitudes of the master (lightly damped) modes only, exists. The theorem then provides an explicit method for calculating it [32, 43]. Applying this method to vibrating systems with nonlinear geometries is discussed in numerous papers [9, 38, 39, 53, 58, 59]. In the conservative case considered here, one can use the center manifold reduction method without making references to slightly and little damped variables. We then simply choose an eigenmode for which we want to extend the invariance property to the nonlinear regime.

Let us now examine the first NNM of the system (8.124): $(X_1, Y_1)$ is chosen arbitrarily as the pair of *master* variables, while $(X_2, Y_2)$ is the so-called pair of *slave* variables. The equation that defines the geometry of the manifold in phase space is obtained through a functional link between master and slave variables. We therefore write:

$$\begin{aligned} X_2 &= u(X_1, Y_1), \\ Y_2 &= v(X_1, Y_1), \end{aligned} \tag{8.125}$$

where $u(X_1, Y_1)$ and $v(X_1, Y_1)$ are the unknown functions to be determined. Equation (8.125) defines a two-dimensional manifold in phase space, and the invariance is ensured by expressing $X_2$ and $Y_2$ as functions of $X_1$ and $Y_1$. To find the unknowns $u$ and $v$, Eq. (8.125) is differentiated with respect to time:

$$\begin{aligned} \dot{X}_2 &= \frac{\partial u}{\partial X_1}\dot{X}_1 + \frac{\partial u}{\partial Y_1}\dot{Y}_1, \\ \dot{Y}_2 &= \frac{\partial v}{\partial X_1}\dot{X}_1 + \frac{\partial v}{\partial Y_1}\dot{Y}_1. \end{aligned} \tag{8.126}$$

Finally, all time derivatives in (8.126) are replaced by their expressions given in (8.124). This leads to a nonlinear equation where the time variable has been removed, and which describes the geometry of the first NNM in phase space:

$$\begin{aligned} v(X_1, Y_1) &= \frac{\partial u}{\partial X_1} Y_1 + \frac{\partial u}{\partial Y_1} f_1(X_1, Y_1, u(X_1, Y_1), v(X_1, Y_1)), \\ f_2(X_1, Y_1, u(X_1, Y_1), v(X_1, Y_1)) &= \frac{\partial v}{\partial X_1} Y_1 + \frac{\partial v}{\partial Y_1} f_1(X_1, Y_1, u(X_1, Y_1), v(X_1, Y_1)). \end{aligned} \tag{8.127}$$

Solving these two partial differential equations yields $u(X_1, Y_1)$ and $v(X_1, Y_1)$, and thus the position of the invariant manifold. The major issue is that the analytical solution of these equations is never known in the general case. Thus, asymptotic or numerical methods are used to determine $u$ and $v$. The dynamics on the manifold is given by replacing $u$ and $v$ by their expressions in (8.124). It can be written with a single oscillator equation, hence giving rise to a reduced-order model. The efficiency of the method might seem relatively insignificant in the particular example treated here, where the reduction of complexity is of only one equation. However, this method yields appreciable results if dynamical systems with a large number $N$ of oscillators can be reduced to one, which is the case when dealing with continuous structures.

The second method is based on the *normal forms* theory. Again, the mathematical tool that is used is very powerful, and is used in almost all branches of physics. The basic ideas of normal forms were developed by Henri Poincaré [55]. The goal is to simplify the dynamics of a system as much as possible, using a well-chosen nonlinear change of variables. In fact, one can show that some nonlinear terms of a dynamical system are essential for obtaining the main features of the dynamics (number and nature of the fixed points, bifurcations), while others can be eliminated without changing its characteristics. These terms, or the so-called non-resonant terms, can be thus eliminated with an appropriate change of variables. Finally, the *normal form* of the system is obtained, that contains the resonant terms only.[18] Returning to our example, we therefore look for a change of variables of the form:

$$\begin{aligned} X_1 &= R_1 + \mathscr{P}_1(R_1, S_1, R_2, S_2), \\ Y_1 &= S_1 + \mathscr{Q}_1(R_1, S_1, R_2, S_2), \\ X_2 &= R_2 + \mathscr{P}_2(R_1, S_1, R_2, S_2), \\ Y_2 &= S_2 + \mathscr{Q}_2(R_1, S_1, R_2, S_2). \end{aligned} \tag{8.128}$$

$(R_1, R_2, S_1, S_2)$ are the new variables, having dimensions of displacements and velocities, respectively. The change of variables is chosen as tangent to the identity:

[18] New results on the use of normal form theory can be found in [41].

the first term indicates that, for small displacements, $R_1 = X_1$, $R_2 = X_2$, $S_1 = Y_1$, and $S_2 = Y_2$, which allows the recovery of the linear results. $\mathscr{P}_1, \mathscr{Q}_1, \mathscr{P}_2, \mathscr{Q}_2$ are unknown functions that are determined iteratively: these quantities are expressed as polynomial functions with unknowns $(R_1, S_1, R_2, S_2)$, whose coefficients are found at each iteration, by eliminating non-resonant terms [37, 66, 70, 71]. Replacing (8.128) in (8.123), one obtains the dynamics expressed in $(R_1, S_1, R_2, S_2)$, i.e., in a curved reference frame generated by the invariant manifolds. In the next step, the appropriate truncations can be made since the invariance is recovered. To study the first NNM, for example, the coordinates corresponding to the second NNM are set equal to zero: $R_2 = S_2 = 0$. After substitution into the last two equations of (8.128), the geometry of the first invariant manifold in phase space is found, which corresponds to Eq. (8.125). Finally, it is found that the dynamics of the first NNM, up to order three, is governed by:

$$\ddot{R}_1 + \omega_1^2 R_1 + \left( \frac{\omega_1^2 + \omega_2^2}{2} + A_1 \right) R_1^3 + B_1 R_1 \dot{R}_1^2 = 0, \tag{8.129}$$

where $A_1$ and $B_1$ arise from the elimination of the non-resonant terms. These coefficients account for the effect of the second linear mode that would have been otherwise abruptly neglected by imposing $X_2 = 0$ in (8.123). These two coefficients are written explicitly:

$$\begin{aligned} A_1 &= -\frac{3\omega_1^2}{2} + \frac{\omega_2^2(2\omega_1^2 - \omega_2^2)}{2(\omega_2^2 - 4\omega_1^2)}, \\ B_1 &= -3 + \frac{\omega_2^2}{\omega_2^2 - 4\omega_1^2}. \end{aligned} \tag{8.130}$$

In total, the nonlinear dynamics is described by a single oscillator, which is able to predict the behavior of the entire system with a good accuracy. It can be shown, for example, that the hardening, resp. softening, behavior of the system, (i.e., the dependence of the frequency with amplitude), is correctly predicted by the dynamics on the manifold (8.129), whereas an erroneous result is obtained if the system (8.123) is simplified in a crude manner by putting $X_2 = 0$ [70].

### 8.7.5 Conclusion

The derivations presented here with the help of a simple system with two degrees of freedom naturally extend to $N$ degrees of freedom, with $N$ arbitrarily large. The influence of damping terms has not been treated, but this question is addressed, for example, in [39, 59] and [66]. Taking also external forces for the calculation of invariant manifolds into account is a more difficult problem, since the invariant manifold then depends on time. One can find an example of such cases in [39].

A nonlinear normal mode (NNM) was defined as an invariant manifold of phase space, tangent at the origin to the corresponding eigenmode, which allows us to consider it as an extension of the eigenmode for which the invariance property is maintained. This property is a key point to adequately reduce nonlinear dynamics. Using NNMs, one can derive reduced-order models, with a small number of degrees of freedom, that contain the main properties of the original dynamics. These methods can be applied to the sound synthesis of nonlinear percussion instruments, in particular. Notice also that the computation of NNMs with application to self-sustained oscillations of the clarinet was made by Noreland et al. [52].

Finally, recent results show that the dynamics of nonlinear thin structures can gain in being examined in light of the wave turbulence theory [36, 72].

## References


1. Amabili, M., Paidoussis, M.P.: Review of studies on geometrically nonlinear vibrations and dynamics of circular cylindrical shells and panels, with and without fluid-structure interaction. ASME Appl. Mech. Rev. **56**(4), 349–381 (2003)
2. Askenfelt, A.: Observations on the transient components of the piano tone. STL-QPSR **34**(4), 15–22 (1993)
3. Atig, M.: Acoustical nonlinearity localised at the open-end of a tube. Measurement, modeling and application to woodwind instruments (in French). Ph.D. thesis, Université du Maine, Laboratoire d'acoustique de l'université du Maine (2004). http://tel.archives-ouvertes.fr/
4. Atig, M., Dalmont, J., Gilbert, J.: Saturation mechanism in clarinet-like instruments, the effect of the localised nonlinear losses. Appl. Acoust. **65**, 1133–1154 (2004)
5. Atig, M., Dalmont, J., Gilbert, J.: Termination impedance of open-ended cylindrical tubes at high sound pressure level. C. R. Acad. Sci. Paris Ser. II **332**, 299–304 (2004)
6. Axisa, F.: Modelling of Mechanical Systems. Discrete Systems, vol. 1. Kogan Page Science, London (2003)
7. Bank, B., Sujbert, L.: Generation of longitudinal vibrations in piano strings: from physics to sound synthesis. J. Acoust. Soc. Am. **117**(4), 2268–2278 (2005)
8. Bilbao, S., O.Thomas, Touzé, C., Ducceschi, M.: Conservative numerical methods for the full von Kármán plate equations. Numer. Methods Partial Differ. Equ. **31(6)**, 1948–1970 (2015)
9. Boivin, N., Pierre, C., Shaw, S.W.: Nonlinear normal modes, invariance, and modal dynamics approximations of non-linear systems. Nonlinear Dyn. **8**(3), 315–346 (1995)
10. Buick, J., Atig, M., Skulina, D., Campbell, D., Dalmont, J., Gilbert, J.: Investigation of non-linear acoustic losses at the open end of a tube. J. Acoust. Soc. Am. **129**, 1261–1272 (2011)
11. Camier, C., Touzé, C., Thomas, O.: Non-linear vibrations of imperfect free-edge circular plates and shells. Eur. J. Mech. A Solids **28**(3), 500–515 (2009)
12. Chabassier, J., Joly, P.: Energy preserving schemes for nonlinear Hamiltonian systems of wave equations. Application to the vibrating piano string. Comput. Methods Appl. Mech. Eng. **199**, 2779–2795 (2010)
13. Chabassier, J., Chaigne, A., Joly, P.: Modeling and simulation of a grand piano. J. Acoust. Soc. Am. **134**(1), 648–665 (2013)
14. Chaigne, A., Touzé, C., Thomas, O.: Nonlinear vibrations in gongs and cymbals. Acoust. Sci. Technol. **26**(5), 403–409 (2005)
15. Conklin, H.A.: Design and tone in the mechanoacoustic piano. Part III. Piano strings and scale design. J. Acoust. Soc. Am. **100**, 1286–1298 (1996)
16. Conklin, H.A.: Piano strings and "phantom" partials. J. Acoust. Soc. Am. **102**(1), 659–659 (1997)

17. Conklin, H.A.: Generation of partials due to nonlinear mixing in a stringed instrument. J. Acoust. Soc. Am. **105**, 536–545 (1999)
18. Coulouvrat, F.: On the equations of nonlinear acoustics. J. Acoust. **5**, 321–359 (1992)
19. Crighton, D.: Nonlinear acoustics. In: Modern Methods in Analytical Acoustics (Lecture Notes). Springer, London (1992)
20. Dalmont, J.P., Nederveen, C.J., Dubos, V., Ollivier, S., Méserette, V., te Sligte, E.: Experimental determination of the equivalent circuit of an open side hole: linear and non linear behaviour. Acustica Acta Acustica **88**, 567–575 (2002)
21. Debut, V., Kergomard, J., Laloë, F.: Analysis and optimisation of the tuning of the twelfths for a clarinet resonator. Appl. Acoust. **66**, 365–409 (2005)
22. Denardo, B.: Nonanalytic nonlinear oscillations: Christiaan Huygens, quadratic Schroedinger equations, and solitary waves. J. Acoust. Soc. Am. **104(3)**, 1289–1300 (1998)
23. Ducceschi, M., Touzé, C.: Modal approach for nonlinear vibrations of damped impacted plates: Application to sound synthesis of gongs and cymbals. J. Sound Vib. **344**, 313–331 (2015)
24. Earnshaw, S.: On the mathematical theory of sound. Philos. Trans. R. Soc. Lond. **150**, 133–148 (1860)
25. Fubini, E.: Anomalies in the propagation of acoustic waves of great amplitude. Alta Frequenza **4**, 530–581 (1935)
26. Galembo, A., Askenfelt, A., Cuddy, L., Russo, F.: Perceptual relevance of inharmonicity and spectral envelope in the piano bass range. Acustica Acta Acustica **90**, 528–536 (2004)
27. Gibiat, V.: Phase space representations of acoustical musical signals. J. Sound Vib. **123**(3), 529–536 (1988)
28. Gilbert, J.: Differences between cylindrical and conical brass instruments; the nonlinear propagation point of view from experiments and simulations. J. Acoust. Soc. Am. **120**, 3332 (2006)
29. Gilbert, J., Kergomard, J., Ngoya, E.: Calculation of the steady-state oscillation of a clarinet using the harmonic balance method. J. Acoust. Soc. Am. **86**, 35–41 (1989)
30. Gilbert, J., Dalmont, J.P., Guimezanes, T.: Nonlinear propagation in woodwinds. In: Proceedings of Forum Acusticum, Budapest (2005)
31. Grassberger, P., Procaccia, I.: Measuring the strangeness of strange attractors. Phys. D **9**, 189–208 (1983)
32. Guckenheimer, J., Holmes, P.: Nonlinear Oscillations, Dynamical Systems and Bifurcations of Vector Fields. Springer, New York (1983)
33. Hamdouni, A., Millet, O.: Classification of thin shell models deduced from the nonlinear three-dimensional elasticity. Part I: the shallow shells. Arch. Mech. **55**(2), 135–175 (2003)
34. Hamilton, M., Blackstock, D. (eds.): Nonlinear Acoustics. Academic Press, New York (1998)
35. Hirschberg, A., Gilbert, J., Msallam, R., Wijnands, A.: Shock waves in trombones. J. Acoust. Soc. Am. **99**, 1754–1758 (1996)
36. Humbert, T., Cadot, O., Düring, G., Josserand, C., Rica, S., Touzé, C.: Wave turbulence in vibrating plates: the effect of damping. Europhys. Lett. **102**(3), 30002 (2013)
37. Jézéquel, L., Lamarque, C.H.: Analysis of nonlinear dynamical systems by the normal form theory. J. Sound Vib. **149**(3), 429–459 (1991)
38. Jiang, D., Pierre, C., Shaw, S.W.: The construction of nonlinear normal modes for systems with internal resonance. Int. J. Nonlinear Mech. **40**(5), 729–746 (2005)
39. Jiang, D., Pierre, C., Shaw, S.W.: Nonlinear normal modes for vibratory systems under harmonic excitation. J. Sound Vib. **288**(4–5), 791–812 (2005)
40. Kantz, H., Schreiber, T.: Nonlinear Time Series Analysis. Cambridge University Press, Cambridge (1997)
41. Lamarque, C.H., Touzé, C., Thomas, O.: An upper bound for validity limits of asymptotic analytical approaches based on normal form theory. Nonlinear Dyn. **70**(3), 1931–1949 (2012)
42. Lyapunov, A.M.: General problem of motion stability (in French). Annales de la faculté des sciences de Toulouse **9**, 203–474 (1907)
43. Manneville, P.: Instabilities, Chaos and Turbulence. Imperial College Press, London (2010)

44. Menguy, L., Gilbert, J.: Gas oscillations in air-filled tubes, solutions and experiments. Acustica Acta Acustica **86**, 798–810 (2000)
45. Monteil, M., Thomas, O., Touzé, C.: Identification of mode couplings in nonlinear vibrations of the steelpan. Appl. Acoust. **89**, 1–15 (2015)
46. Morse, P.M.: Vibration and Sound. Acoustical Society of America, Melville (1981)
47. Msallam, R., Dequidt, S., Caussé, R., Tassart, S.: Physical model of the trombone including nonlinear effects; application to the sound synthesis of loud tones. Acustica Acta Acustica **86**, 725–736 (2000)
48. Müller, G., Lauterborn, W.: The bowed string as a nonlinear dynamical system. Acustica Acta Acustica **82**(4), 657–664 (1996)
49. Murthy, G.S.S., Ramakrishna, B.S.: Nonlinear character of resonance in stretched strings. J. Acoust. Soc. Am. **38**, 461–471 (1965)
50. Myers, A., Pyle, R., Gilbert, J., Campbell, D., Chick, J., Logie, S.: Effects of nonlinear sound propagation on the characteristic timbres of brass instruments. J. Acoust. Soc. Am. **131**, 678–688 (2012)
51. Nayfeh, A.H., Mook, D.T.: Nonlinear Oscillations. Wiley, New York (1979)
52. Noreland, D., Bellizzi, S., Bouc, R., Vergez, C.: Nonlinear modes of clarinet-like musical instruments. J. Sound Vib. **324**, 983–1002 (2006)
53. Peshek, E., Pierre, C., Shaw, S.: A new galerkin-based approach for accurate non-linear normal modes through invariant manifolds. J. Sound Vib. **249**(5), 971–993 (2002)
54. Pierce, A.D.: Acoustics: An Introduction to Its Physical Principles and Applications. Acoustical Society of America, Melville (1989)
55. Poincaré, H.: Sur les propriétés des fonctions définies par les équations aux différences partielles. Gauthier-Villars, Paris (1879)
56. Rosenberg, R.M.: On non-linear vibrations of systems with many degrees of freedom. Adv. Appl. Mech. **9**, 155–242 (1966)
57. Rudenko, O., Soluyan, S.: Theoretical Foundations of Nonlinear Acoustics. Consultant Bureau, New York (1977)
58. Shaw, S.W., Pierre, C.: Nonlinear normal modes and invariant manifolds. J. Sound Vib. **150**(1), 170–173 (1991)
59. Shaw, S.W., Pierre, C.: Normal modes for nonlinear vibratory systems. J. Sound Vib. **164**(1), 85–124 (1993)
60. Thomas, O.: Analysis and modeling of nonlinearly vibrating thin elastic structures. Application to percussion instruments (in French). Ph.D. thesis, Telecom ParisTech (2001). https://hal.archives-ouvertes.fr/
61. Thomas, O., Bilbao, S.: Geometrically non-linear flexural vibrations of plates: in-plane boundary conditions and some symmetry properties. J. Sound Vib. **315**(3), 569–590 (2008)
62. Thomas, O., Touzé, C., Chaigne, A.: Nonlinear behavior of gongs through the dynamics of simple rods systems. In: Bonsi, D. (ed.) Proceedings of the International Symposium on Musical Acoustics, vol. 1, pp. 173–178, Perugia (2001)
63. Thomas, O., Touzé, C., Chaigne, A.: Non-linear vibrations of free-edge thin spherical shells: modal interaction rules and 1:1:2 internal resonance. Int. J. Solid Struct. **42**(1), 3339–3373 (2005)
64. Thomas, O., Touzé, C., Luminais, E.: Non-linear vibrations of free-edge thin spherical shells: experiments on a 1:1:2 internal resonance. Nonlinear Dyn. **49**(1–2), 259–284 (2007)
65. Thompson, M., Strong, W.: Inclusion of wave steepening in a frequency-domain model of trombone sound production. J. Acoust. Soc. Am. **110**, 556–562 (2001)
66. Touzé, C., Amabili, M.: Nonlinear normal modes for damped geometrically nonlinear systems: application to reduced-order modeling of harmonically forced structures. J. Sound Vib. **298**(4–5), 958–981 (2006)
67. Touzé, C., Chaigne, A.: Lyapunov exponents from experimental time series: application to cymbal vibrations. Acustica Acta Acustica **86**, 557–567 (2000)
68. Touzé, C., Thomas, O.: Non-linear behaviour of free-edge shallow spherical shells: effect of the geometry. Int. J. Nonlinear Mech. **41**(5), 678–692 (2006)

69. Touzé, C., Thomas, O., Amabili, M.: Transition to chaotic vibrations for harmonically forced perfect and imperfect circular plates. Int. J. Nonlinear Mech. **46**(1), 234–246 (2011)
70. Touzé, C., Thomas, O., Chaigne, A.: Hardening/softening behaviour in nonlinear oscillations of structural systems using non-linear normal modes. J. Sound Vib. **273**(1–2), 77–101 (2004)
71. Touzé, C., Thomas, O., Huberdeau, A.: Asymptotic nonlinear normal modes for large-amplitude vibrations of continuous structures. Comput. Struct. **82**(31–32), 2671–2682 (2004)
72. Touzé, C., Bilbao, S., Cadot, O.: Transition scenario to turbulence in thin vibrating plates. J. Sound Vib. **331**(2), 412–433 (2012)
73. Valette, C.: The mechanics of vibrating strings. In: Hirschberg, A., Kergomard, J., Weinreich, G. (eds.) Mechanics of Musical Instruments. CISM Courses and Lectures, vol. 355, pp. 115–183. Springer, Wien (1995)
74. Vergez, C., Rodet, X.: New algorithm for nonlinear propagation of a sound wave. Application to a physical model of a trumpet. J. Signal Process. **4**, 79–87 (2000)
75. Watzky, A.: Non-linear three-dimensional large-amplitude damped free vibration of a stiff elastic string. J. Sound Vib. **153**(1), 125–142 (1992)